JAERI-Research
95-056

BENCHMARK PROBLEM FOR IAEA COORDINATED RESEARCH PROGRAM (CRP-3) ON GCR AFTERHEAT REMOVAL (I)

August 1995

Shoji TAKADA, Yasuaki SHIINA, Yoshiyuki INAGAKI
Makoto HISHIDA and Yukio SUDO

日本原子力研究所
Japan Atomic Energy Research Institute

本レポートは，日本原子力研究所が不定期に公刊している研究報告書です。
入手の問合わせは，日本原子力研究所技術情報部情報資料課（〒319-11 茨城県那珂郡東海村）あて，お申し越しください。なお，このほかに財団法人原子力弘済会資料センター（〒319-11 茨城県那珂郡東海村日本原子力研究所内）で複写による実費頒布をおこなっております。

This report is issued irregularly.
Inquiries about availability of the reports should be addressed to Information Division, Department of Technical Information, Japan Atomic Energy Research Institute, Tokai-mura, Naka-gun, Ibaraki-ken 319-11, Japan.

編集兼発行　日本原子力研究所
印　　刷　㈱原子力資料サービス

Benchmark Problem for IAEA Coordinated Research Program (CRP-3) on GCR Afterheat Removal(Ⅰ)

Shoji TAKADA, Yasuaki SHIINA, Yoshiyuki INAGAKI
Makoto HISHIDA and Yukio SUDO

Department of High Temperature Engineering
Tokai Research Establishment
Japan Atomic Energy Research Institute
Tokai-mura, Naka-gun, Ibaraki-ken

(Received July 26, 1995)

In this report, detailed data which are necessary for the benchmark analysis of International Atomic Energy Agency (IAEA) Coordinated Research Program (CRP-3) on "Heat Transport and Afterheat Removal for Gas-cooled Reactors under Accident Conditions" are described concerning about the configuration and sizes of the cooling panel test apparatus, experimental data and thermal properties.

The test section of the test apparatus is composed of pressure vessel (max. 450℃) containing an electric heater (max. 100kW, 600℃)and cooling panels surrounding the pressure vessel. Gas pressure is varied from vacuum to 1.0MPa in the pressure vessel.

Two experimental cases are selected as benchmark problems about afterheat removal of HTGR, described as follows,

The experimental conditions are vacuum inside the pressure vessel and heater output 13.14kW, and helium gas pressure 0.73MPa inside the pressure vessel and heater output 28.79kW. Benchmark problems are to calculate temperature distrbutions on the outer surface of pressure vessel and heat transferred to the cooling panel using the experimental data.

The analytical result of temperature distribution on the pressure vessel was estimated +38℃, -29 ℃ compared with the experimental data, and analytical result of heat transferred from the surface of pressure vessel to the cooling panel was estimated max. -11.4% compared with the experimental result by using

the computational code -THANPACST2- of JAERI.

Keywords: IAEA, Benchmark Problem, Afterheat Removal, HTGR, Passive Cooling System, Heat Transfer, Radiation, Natural Convection, Accident, Reactor Cavity Cooling System, Coolling Panel System, Surface Cooler System

ＩＡＥＡのＣＲＰ－３における高温ガス炉崩壊熱除去に関するベンチマーク問題（Ｉ）

日本原子力研究所東海研究所高温工学部
高田　昌二・椎名　保顕・稲垣　嘉之
菱田　　誠・数土　幸夫

（1995年７月26日受理）

国際原子力機関（International Atomic Energy Agency : IAEA)の高温ガス炉事故時における崩壊熱除去に関する国際協力研究(Coordinated Research Program : CRP-3)に必要なベンチマーク問題について，冷却パネル特性試験装置の詳細と実験データに基づき作成したベンチマーク問題を報告するとともに，数値解析コード-THANPACST2-により得られた数値解析結果を述べる。

冷却パネル特性試験装置の試験部は，100ｋＷのヒーターを内蔵する圧力容器と，容器を取り囲む水冷管からなる冷却パネルから構成されており，最高負荷圧力 1.0ＭＰａ，ヒーター最高温度600℃，圧力容器表面最高温度450℃の性能を有する。

崩壊熱除去に関するベンチマーク問題では，圧力容器内真空，ヒーター出力 13.14ｋＷの条件及び圧力容器内ヘリウムガス圧力が0.73ＭＰａ，ヒーター出力が 28.79ｋＷの条件で得られた実測値を用いて，圧力容器表面の温度分布と圧力容器から冷却パネルへの除熱量を計算する。原研の-THANPACST2-による圧力容器表面温度の数値解析結果は実験値に対して最高＋38℃，－29℃の精度で，また，圧力容器から冷却パネルへの除熱量の数値解析結果はヒータ出力の実験値に対して最高－11.4％の精度で予測が可能であった。

東海研究所：〒319-11　茨城県那珂郡東海村白方白根２－４

Contents

目　　次

1. INTRODUCTION

International Atomic Energy Agency (IAEA) Coordinated Research Program (CRP) on "Heat Transport and Afterheat Removal for Gas-cooled Reactors under Accident Conditions" started at November, 1993. In this program, benchmark tasks were proposed for the analysis of passive afterheat removal from gas-cooled reactors (GCR) under accident conditions.

Specific objective of the benchmark program is to capture the essential heat transfer features of reactor-to-reactor vessel cooling system (VCS) and provide useful information applicable to a wide variety of designs, operating conditions and model parameters. The exercise would result in partial validation and verification of the analytical tools used for GCR applications. Sensitivity studies would be used to determine the relative importance of selected design features and to investigate the effects of changing various modeling options and parameters.

The comparisons of various analytical techniques and approximation methods with each other and with the experimental data should prove to be useful. Hence, verification and validation (V&V) of both the VCS design features and the analytical methods used to predict behavior should be derivable from the fact that an international variety of analytical approaches used by the participants and that the corroborating experimental data are in agreement.

Other objectives should include: 1) evidence of the advantages of some design choices over others; and 2) indications of how the reactor vessel and VCS can be monitored during normal operation so that problems potentially affecting performance during an accident condition can be detected.

Specific benefits expected through the exercises of this program are described as follows,

(1) Determination of the relative accuracy and cost effectiveness of using 1- or 2- vs 3-dimensional analysis for various aspects and conditions of the accident scenarios (for radiant and convective heat transfer). The combination of the analytical and experimental validation exercises should help to determine the degree of complexity required to analyze passive decay heat removal phenomena with a given accuracy.

(2) Accuracy, applicability, and importance of candidate correlations for various elements of the analysis. (Example: the correlation for convective heat transfer in the reactor vessel-to-VCS cavity for various vessel and VCS temperature distribution scenarios.)

(3) Predictability of VCS heat rejection, vessel temperature distributions, hot spots for VCS asymmetries, and performance degradation (e.g., due to reduced emissivity or panel partial failures, and top head penetrations - such as control rod drive tubes might be crucial and difficult to predict.

(4) Effects of participating media (e.g., steam) in the vessel-to-VCS on radiant heat transfer.

(5) Some practical aspects of VCS design and operation would probably become apparent to CRP participants from their involvement in the experimental validation work.

An important point in formulation of the benchmark problem is the fact that time response of the reactor internals during conduction cooldown accidents (one of the limiting accident conditions is referred to as a "conduction cooldown" accident) is much slower than that for the heat removal process of the VCS. Hence, if the temperature profiles are established for the reactor vessel, the calculation of cooling performance of the passive cooling system can be treated as a steady state problem. Therefore, experimental

data of cooling performance of the cooling panel test apparatus (Japan Atomic Energy Research Institute: JAERI, JAPAN) investigating heat transfer performance of the cooling panel system was selected as the benchmark problem between computational codes and experimental data.

The computational code -THANPACST2- [1], which can calculate the flow and temperature distribution with thermal conduction, radiation and natural convection, was applied to the benchmark problem.

This report describes detailed data which are necessary for the benchmark analysis: configuration and sizes of the experimental apparatus, experimental data and thermal properties. And the analytical results using the computational code -THANPACST2- were compared with the experimental results to verify the analytical method and model.

2. EXPERIMENTAL APPARATUS

2.1 Test apparatus of cooling panel system

Schematic diagrams of the apparatus and detailed configurations of the components are shown in Figs. 2.1～2.18. Materials and thermophysical properties of the components are shown in Tables 2.2 and 2.3.

A flowsheet of the test apparatus of cooling panel is shown in Fig. 2.1. The test apparatus consists of a test section and systems for water supply, helium gas supply and for vacuum. The test section is composed of a pressure vessel containing a heater and cooling panels surrounding the pressure vessel as shown in Fig. 2.2.

The pressure vessel is divided into upper head, shell, lower head, legs and skirt. Main specifications of the pressure vessel are described as follows,

Height of the pressure vessel	: 3000mm,
Inner diameter of the shell	: 1000mm,
Thickness	: 12mm,
Radius of the upper head	: 500mm,
Configuration of the lower head	: 2 : 1 half ellipsoid,
Longer radius of the lower head	: 500mm,
Shorter radius of the lower head	: 250mm,
Working fluid	: Helium and Nitrogen gas,
Pressure	: 1.3Pa～1.0MPa.

The upper head is connected with the shell of the pressure vessel by a flange as shown in Fig. 2.3. Detailed sizes and configuration of the flange is shown in Fig. 2.4. The pressure vessel is supported by four legs, and four boards attached between the legs to simulate the skirt type support as shown in Fig. 2.5～2.7. The pressure of working fluid is varied from vacuum (1.3Pa) to 1.0MPa to investigate the effects of gas pressure which affects the natural convection in the pressure vessel. Helium and nitrogen gas are used as working fluids in the pressure vessel.

The heater in the pressure vessel simulates reactor core as shown in Fig. 2.8. Main specifications of the electric heater are described as follows,

Height	: 2000mm,
Diameter	: 600mm,
Maximum temperature	: 600℃,
Maximum total power	: 100kW,
Maximum output power of heater segment No. 1	: 7kW,
Maximum output power of heater segments No. 2-No. 5	: 21kW,

Maximum output power of heater segment No. 6	: 7kW,
Heat transfer area of heater segment No. 1	: 0.283m^2,
Heat transfer area of heater segments No. 2-No. 5	: 0.848m^2,
Heat transfer area of heater segment No. 6	: 0.135m^2.

The heater is divided into 6 segments. Each heater segment consists of an annular type ceramic block filled with thermal insulator and nichrome helical coils wound around the block. The heater is supported by a heater support composed of 8 legs and an annular plate as shown in Fig. 2.9.

The cooling panels which consist of cooling tubes are installed around the pressure vessel to remove the heat from the pressure vessel. The cooling panel is composed of three parts: the upper, side and lower cooling panels. Each cooling panel has 25, 88 and 12 cooling tubes, respectively. Figure 2.10 shows the upper, side and lower cooling panels. Main specifications of the cooling panels are described as follows,

Outer diameter of the cooling tube	: 31.8mm,
Pitch of the cooling tubes	: 60mm,
(the length between the center lines of cooling tubes),	
Maximum flow rate of water	: 10m^3/h.

The cooling tubes are connected with two ring type headers. Cooling water is supplied from two water supply systems. In order to unify the emissivity, black paint is coated on the outer surfaces of cooling tubes and the pressure vessel.

Thermal insulator made of KAOWOOL (ceramic fiber insulator) surrounds outside of the cooling panels. Main specifications of the insulator are described as follows,

Outer diameter	: 2210mm,
Height	: 4000mm,
Thickness	: 100mm.

In the test section, the cooling panel removes the heat from the heater with thermal radiation and natural convection of helium gas (inside the pressure vessel) and the air(outside).

Temperatures of the surfaces of the pressure vessel, the heater, the cooling tubes and the insulator are measured by sheathed chromel-alumel thermocouples.

Outer surface temperature of the pressure vessel was measured on four different angles at 90° intervals around the surface as shown in Fig. 2.11. All thermocouples are divided into 7 groups from A to K and the thermocouples in each groups are numbered by tag number. Attached positions, groups and tag numbers of the thermocouples are shown in Table 2.1 and Figs. 2.12～2.18. Detailed positions of the measuring points of temperatures on the shell, upper head and lower head of the pressure vessel are shown in Figs. 2.12, 2.13 and 2.14, respectively.

Figure 2.15 shows the measuring points of the temperatures on the heater, of working fluid in the

pressure vessel, and on the inner surface of the pressure vessel.

Detailed positions of the measuring points of temperatures on the middle 4 heater segments are shown in Fig. 2.16. Thermocouples are attached on the thermocouple holders which are vertically connected between the heater support plate and upper plate of the heater.

Detailed positions of the measuring points of temperatures on the top and bottom heater segments are shown in Fig. 2.17. Thermocouples are attached on the holders which are horizontally connected with the top and bottom annular plates.

Temperatures of helium gas are measured by sheathed chromel-alumel thermocouples. Detailed positions of the measuring points of gas temperatures inside the pressure vessel are shown in Fig. 2.18. Thermocouples are held by thermocouple holders connected to the upper plate of the heater. Radiation preventing plates are installed between the tips of the thermocouples and the heater.

In addition, temperatures of cooling water are measured by platinum resistance bulbs and the flow rate of the water in cooling tubes are measured by magnetic flowmeters as shown in Fig. 2.1. Electric powers of heater segments are measured by power transducers. Heat removed by the cooling panel is calculated from the enthalpy rise of cooling water.

Table 2.1 shows the correspondence of the tag numbers to measuring items in the experimental apparatus.

2. 2 Thermophysical properties

Tables 2.2 and 2.3 show thermophysical properties of the materials used in the test apparatus. Table 2.2 shows thermal conductivities[2]. Table 2.3 shows emissivities of the heater (nichrome coil and ceramic blocks) and pressure vessel taken from reference[3].

In the vacuum experiments, emissivities of the components were measured to compare with the values given in the reference. Heat transferred by thermal radiation from the heater surface to the pressure vessel are expressed as follows by assuming infinite concentric cylinders,

$$q=A_1\cdot\epsilon\cdot\sigma\cdot(T_1^4-T_2^4) \qquad [2.1]$$

$$\epsilon=\frac{1}{\frac{1}{\epsilon_1}+\frac{A_1}{A_2}\cdot(\frac{1}{\epsilon_2}-1)} \qquad [2.2]$$

q : Output power of the heater,

A_1 : area of the surface of the heater,

A_2 : area of the surface of the pressure vessel,

ϵ_1 : emissivity of the surface of the heater,

ε_2 : emissivity of the surface of the pressure vessel,
σ : Stefan-Boltzmann constant,
T_1 : surface temperature of the heater,
T_2 : surface temperature of the pressure vessel.

Emissivities are calculated by using temperatures and heat flux as shown in Table 2.4. Emissivity of the surface of the pressure vessel is assumed to be constant: ε_2=0.79. Emissivities of the heater depend on temperature and are distributed between the values of polished and oxidized nichrome in the reference. Therefore, experimental values of emissivities are considered to be reasonable.

The outer surfaces of pressure vessel, cooling tubes and inner surface of insulator are uniformly coated by black paint to unify the emissivities. Emissivities of the outer surface of the pressure vessel are assumed to be 0.95.

3. BENCHMARK PROBLEM

Two experiments are selected as benchmark problems. The first is the case of vacuum condition to eliminate the effect of natural convection in the pressure vessel. The second is the case of helium gas condition to investigate heat transfer performance with natural convection in the pressure vessel.

3. 1 Experimental data

3. 1. 1 Vacuum condition

Experimental data are shown in Table 3.1. Output power of the heater and pressure in the pressure vessel are described as follows,

Pressure in the pressure vessel : 1.3Pa,
Total heater output power : 13.14kW,
Output power (Heat flux) of heater segment No. 1 : 1.010kW (3.569kW/m^2),
Output power (Heat flux) of heater segment No. 2 : 2.306kW (2.719kW/m^2),
Output power (Heat flux) of heater segment No. 3 : 2.636kW (3.108kW/m^2),
Output power (Heat flux) of heater segment No. 4 : 2.460kW (2.901kW/m^2),
Output power (Heat flux) of heater segment No. 5 : 3.763kW (4.438kW/m^2),
Output power (Heat flux) of heater segment No. 6 : 0.964kW (7.141kW/m^2),

ε_2 : emissivity of the surface of the pressure vessel,
σ : Stefan-Boltzmann constant,
T_1 : surface temperature of the heater,
T_2 : surface temperature of the pressure vessel.

Emissivities are calculated by using temperatures and heat flux as shown in Table 2.4. Emissivity of the surface of the pressure vessel is assumed to be constant: ε_2=0.79. Emissivities of the heater depend on temperature and are distributed between the values of polished and oxidized nichrome in the reference. Therefore, experimental values of emissivities are considered to be reasonable.

The outer surfaces of pressure vessel, cooling tubes and inner surface of insulator are uniformly coated by black paint to unify the emissivities. Emissivities of the outer surface of the pressure vessel are assumed to be 0.95.

3. BENCHMARK PROBLEM

Two experiments are selected as benchmark problems. The first is the case of vacuum condition to eliminate the effect of natural convection in the pressure vessel. The second is the case of helium gas condition to investigate heat transfer performance with natural convection in the pressure vessel.

3. 1 Experimental data

3. 1. 1 Vacuum condition

Experimental data are shown in Table 3.1. Output power of the heater and pressure in the pressure vessel are described as follows,

Pressure in the pressure vessel : 1.3Pa,
Total heater output power : 13.14kW,
Output power (Heat flux) of heater segment No. 1 : 1.010kW (3.569kW/m^2),
Output power (Heat flux) of heater segment No. 2 : 2.306kW (2.719kW/m^2),
Output power (Heat flux) of heater segment No. 3 : 2.636kW (3.108kW/m^2),
Output power (Heat flux) of heater segment No. 4 : 2.460kW (2.901kW/m^2),
Output power (Heat flux) of heater segment No. 5 : 3.763kW (4.438kW/m^2),
Output power (Heat flux) of heater segment No. 6 : 0.964kW (7.141kW/m^2),

3. 1. 2 Helium gas condition

Experimental data are shown in Table 3.2. Output power of the heater and pressure in the pressure vessel are described as follows,

Pressure in the pressure vessel : 0.73MPa,
Total heater output power : 28.79kW,
Output power (Heat flux) of heater segment No. 1 : 1.157kW (4.088kW/m^2),
Output power (Heat flux) of heater segment No. 2 : 3.106kW (3.663kW/m^2),
Output power (Heat flux) of heater segment No. 3 : 3.524kW (4.156kW/m^2),
Output power (Heat flux) of heater segment No. 4 : 5.096kW (6.009kW/m^2),
Output power (Heat flux) of heater segment No. 5 : 10.42kW (12.29kW/m^2),
Output power (Heat flux) of heater segment No. 6 : 5.492kW (40.68kW/m^2),

3.2 Benchmark problems

The benchmark problems are,
(1) to calculate the temperature distributions on the outer surface of the pressure vessel and to calculate the heat transferred from the pressure vessel to the cooling panels under the boundary conditions of the output power of the heater and the pressure in the pressure vessel given in 3.1.1. and 3.1.2., and the cooling panel temperatures, F01 to F12, given in Tables 3.1 and 3.2.

(2) to calculate the heat transferred from the pressure vessel to the cooling panels under boundary conditions of the temperature distribution on the outer surface of the pressure vessel, A01～A50, B01～B23, C01～C29 and D01～D33, given in Tables 3.1 and 3.2, and the cooling panel temperatures, F01～F12, given in Tables 3.1 and 3.2.

We propose all the participants solve the problem (1). We provided the problem (2) for checking the results of the problem (1).

4. ANALYTICAL METHOD

4. 1 Computational code

The analytical code -THANPACST2- is a two-dimensional time dependent flow and heat transfer code and it is able to calculate both the flow and the temperature distribution of the components with thermal radiation, conduction and natural convection. The staggered grid system is used to describe the field variables such as temperature and pressure at the center of a cell and the flow variables (velocities) at the surface.

A heat transfer coefficient between the surface of a component cell and fluid is given as a constant local Nusselt number Nu_c for each surface of component cell. And each Nusselt number Nu_c is calculated from mean Nusselt number Nu_m which is acquired from an empirical equation of natural convection corresponding to the configuration of component cell and fluid.

For the flow calculation, the upwind scheme and the pressure correction method are used to determine the variables on the finite-volume faces and nodes. The buoyancy force is calculated by Boussinesq's approximation. The properties of the fluid, such as density, viscosity, thermal conductivity and Plandtl number, are obtained as the function of temperature and pressure. Thermal conductivities of components are assumed to be constant.

The surface temperatures of nodes are acquired by considering the balance of the heat transferred with thermal radiation from surface 1 to surface 2, and the emissivity ε applied to concentric cylinders and spheres are defined as follows,

$$Q_{12}=A_1 \cdot \varepsilon \cdot \sigma \cdot F_{12} \cdot (T_1^4-T_2^4)^{(4)}, \qquad [4.1]$$

$$\varepsilon = 1/(1/\varepsilon_1 + A_1/A_2 \cdot (1/\varepsilon_2 - 1)), \qquad [4.2]$$

A_1 : area of surface 1 (inner cylinder or sphere),

A_2 : area of surface 2 (outer cylinder or sphere),

ε_1, ε_2 : emissivities of surfaces 1, 2,

σ : Stefan-Boltzmann constant,

T_1, T_2 : Surface temperatures of surfaces 1, 2.

Geometric factor F_{12} for each surface is obtained by using the unit-sphere method[3]. It is possible in the code to consider heat transferred with thermal radiation between a face and maximum 30 faces.

4. 2 Analytical model

Figure 4.1 shows the differential scheme which simulates the experimental model. The two-dimensional cylindrical geometry (a 23 × 39 grid system) is used in consideration of the arrangement of the heater, pressure vessel and cooling panel supported by skirt type support.

There are air flow channels between the cavity which is surrounded by lower head of the pressure

vessel and skirt type support and the cavity outside of the pressure vessel. The cavities are connected with clearances between the ground and skirt type support, and flow paths in H-type legs. The air channels are expressed by porous body cells which have properties of both solid and fluid cells at the upper and lower edges of skirt type support in the analytical model.

Outside of the cooling panel is assumed to be insulated and all the heat is transferred from pressure vessel to cooling tubes, and heat loss from the insulator to the outside is assumed to be zero.

Thermal radiation is assumed to be exchanged between pressure vessel and surfaces of electric heater, cooling panel and skirt type support, and also between cooling panel and skirt type support.

Natural convection heat transfer coefficients between the outer surface of shell of pressure vessel and side cooling panel (region ① in Fig. 2.2) and between the side surface of heater and the inner surface of pressure vessel(②) are calculated from the empirical correlation,

$$Nu_m=0.286\cdot Ra^{0.258}\cdot Pr^{0.006}\cdot H^{-0.238}\cdot K^{-0.442}, \qquad [4.3]$$

H: Aspect ratio,

K: Ratio of outer and inner radii of cylinders,

Pr: Prantdl number,

Ra: Rayleigh number (=Gr· Pr),

Gr: Grashof number,

for the case of a concentric cylinder (inner surface heated, and outer surface cooled) by Thomas and de Vahl Davis[5]. Natural convection heat transfer coefficients for the top surface of heater (③), upper cooling panel (④) and outer surface of upper head of pressure vessel (⑤) are calculated from the empirical correlation,

$$Nu_m=0.54\cdot Ra^{0.25} \qquad (1\times10^5<Ra<2\times10^7), \qquad [4.4]$$

$$Nu_m=0.14\cdot Ra^{0.33} \qquad (2\times10^7<Ra<3\times10^{10}),$$

for the cases of horizontal surfaces heating above or cooling below by Fishenden and Saunders[6]. Natural convection heat transfer coefficients for the inner surface of upper head of pressure vessel (⑥) is calculated from the empirical correlations by Shiina[7],

$$Nu_m=0.1974\cdot Ra^{0.25} \qquad (1.0\times10^6<Ra<1.0\times10^9), \qquad [4.5]$$

$$Nu_m=0.312\cdot Ra^{0.33} \qquad (1.0\times10^9<Ra<5.5\times10^{10}).$$

Natural convection heat transfer coefficients for the bottom surface of heater (⑦), inner surface of lower head of pressure vessel (⑧) and lower cooling panel (⑨) are calculated from the empirical correlation,

$$Nu_m=0.27\cdot Ra^{0.25}, \qquad [4.6]$$

for the cases of horizontal surfaces heating below and cooling above by Fishenden and Saunders[5]. Natural convection heat transfer coefficient for the outer surface of lower head of pressure vessel (⑩) is obtained from Nu_c=45 which is calculated from experimental results of vacuum condition inside the pressure vessel, because the configuration of the lower head of the pressure vessel is half-ellipsoid and there is no empirical correlation for this configuration. Mean Nusselt numbers used for each regions are summarized in Table 4.1.

4.3 Analytical conditions

In the analysis, the temperature distributions on the outer surface of pressure vessel and the heat transferred from the pressure vessel to the cooling panels are calculated under the boundary conditions described in 3-2 (1). Emissivity of heater is varied from 0.40 to 0.80 as a parameter. Emissivities of surfaces of cooling panel, inner and outer surfaces of pressure vessel and skirt type support are adopted as 0.95, 0.79, 0.95 and 0.95, respectively.

The heat transferred from the pressure vessel to the cooling panels is calculated under boundary conditions described in 3-2 (2). Emissivities of surfaces of cooling panel, outer surfaces of pressure vessel and skirt type support are varied from 0 to 1.00 to investigate the emissivity dependence of thermal radiation heat transfer.

5. COMPARISON BETWEEN EXPERIMENTAL AND ANALYTICAL RESULTS

5.1 Benchmark problem (1)

5. 1. 1 Vacuum condition inside the pressure vessel

Experimental and analytical results of temperature distribution of the components and heat flux distribution of the heater are shown in Fig. 5.1. Analytical results of temperatures on the pressure vessel don't depend on emissivity of the heater. Experimental results show that temperatures around the flange and the connecting regions between legs and shell of pressure vessel show lower values. Temperatures are almost uniform on the shell of pressure vessel. Analytical results of temperature distribution on the pressure vessel agree with experimental results except the middle part of upper head and the connecting regions between legs and shell of pressure vessel.

Analytical results of temperature at the middle part of upper head is about 17℃ lower than experimental one. Since the area of the upper head in the analytical model is about 1.2 times larger than experimental apparatus, it is considered that the heat transferred from the upper head is over estimated and temperatures on the upper head show lower values.

Temperature on the connecting region between legs and shell of pressure vessel is 38℃ higher than experimental one. The reasons would be that the heat transfer area around the connecting region of the shell of pressure vessel and legs are estimated smaller than the ones of experimental apparatus, and that there are air channels between inside and outside of skirt through H-type legs.

On the other hand, analytical results of temperature on heater increases as emissivity of heater decreases, and the analytical results in the case of emissivity ε =0.66 agree with experimental results except temperatures on heater segment No. 5. Temperature on the heater segment No. 5 is 103℃ higher than experimental one. The reason would be that heat removed from segment No. 5 is small because the segment is faced to the high temperature connecting regions.

Analytical results of temperature contour and velocity vector map are shown in Fig. 5.2. Temperature gradient is steep around the pressure vessel as shown in the figure. Air flowing up on the shell of pressure vessel is partially disturbed by the flange. Air heated by the pressure vessel flows upward and is cooled and turns at the upper cooling panel. And the air is cooled and flows downward along the side cooling panel. The air heated up below the lower head of pressure vessel flows up through the channels between H-type beam legs and pressure vessel, and the legs and connecting regions of pressure vessel are cooled by the air flow. Its effect on the temperature distribution around the area is not negligible as mentioned above.

5. 1. 2 Helium gas condition inside the pressure vessel

Experimental and analytical results of temperature distribution of the components and heat flux distribution of the heater are shown in Fig. 5.3. Temperatures around the flange and connecting regions

between legs and shell of pressure vessel show lower values. Temperatures are almost uniform on the shell of pressure vessel. Analytical results of pressure vessel agree with experimental results except the top of upper head and the connecting regions between legs and shell of pressure vessel. Analytical result of temperature on the top of upper head of pressure vessel is 29℃ lower than experimental one. Analytical results of temperature and velocity vector map are shown in Fig. 5.4. Analytical result of helium gas temperature is 70℃ lower than experimental one at measuring point of E26. High temperature gas flow along the side wall of the heater would be prevented in the analysis by the stepwise wall which simulates the inner wall of upper head of pressure vessel. This would be one reason of the low temperature in the analysis. One more reason would be that the area of the upper head in the analytical model is 1.2 times larger than experimental apparatus.

On the other hand, analytical results of temperatures on heater agree with experimental ones except the ones on heater segments No.5 and 6. Temperatures on the heater segments No. 5 and 6 are max. 220℃ higher than experimental ones. And temperatures on the connecting regions are max. 37℃ higher than experimental ones. This would yield high temperature of heater segment No. 5 described in previous section. And it is also considered that temperature of heater is higher than measured value because thermocouples which measure temperatures of heater don't contact with heater segments. Thermo-couples of No. 5 and 6 heater segments are set in low temperature helium gas flow.

Analytical result of heat transferred with thermal radiation is 60.1% of the total heat transferred from heater.

5. 2 Benchmark problem (2)

Total heat transferred from the pressure vessel to the cooling panel are investigated varying emissivity of the outer surface of pressure vessel from 0 to 1.00. Results are shown in Fig. 5.5. Analytical results employing the emissivity of outer surface of pressure vessel $\varepsilon_{p.v}$=0.95 lies between the two values which are total heat input and heat transferred to the cooling panel. Hence, the differences between total heat input and heat transferred to the cooling panel in vacuum and helium gas conditions are 14.6 and 13.4% of total heat input, respectively, and they are considered to be heat loss from the insulator.

The analytical results of relationship between emissivity and ratio of thermal radiation to total heat transferred to the cooling panel is shown in Fig. 5.6. The ratios of thermal radiation to total heat transferred to the cooling panel in the case of $\varepsilon_{p.v}$=0.95 are 71.0 and 74.4% for vacuum and helium gas conditions, respectively.

6. CONCLUSION

International Atomic Energy Agency (IAEA) Coordinated Research Program (CRP) on "Heat Transport and Afterheat Removal for Gas-cooled Reactors under Accident Conditions" started at November, 1993. In this program, benchmark tasks were proposed for the analysis of passive afterheat removal from gas-cooled reactors (GCR) under accident conditions. The experimental data of cooling performance of the cooling panel test apparatus (Japan Atomic Energy Research Institute: JAERI, JAPAN) investigating heat transfer performance of the cooling panel system was selected as the benchmark problem between computational codes and experimental data. This report describes detailed data which are necessary for the benchmark analysis: configuration and sizes of the experimental apparatus, experimental data and thermal properties. And the analytical results using the computational code -THANPACST2- of JAERI were compared with the experimental results to verify the analytical method and model. Conclusions are summarized as follows,

(1) Analytical results of temperature distribution on the pressure vessel are independent of emissivity of heater under the given boundary conditions of heat input and cooling panel temperature.

(2) Analytical results of temperature distribution of the shell of pressure vessel agree with experimental results.

(3) Analytical results of temperatures on the upper head of pressure vessel show lower values than experimental results. This would be caused by the reasons that in the analysis the area of upper head of pressure vessel is set 1.2 times larger than the actual area and the surface of upper head is a stepwise wall and not smooth which prevents the hot helium gas flow inside the upper head of pressure vessel.

(4) Analytical results of temperatures around the connecting region between legs and shell of pressure vessel in the analysis show higher value than experimental results. This would be caused by the reasons that in the analysis the heat transfer areas around the connecting regions of the shell of pressure vessel and legs are set smaller than the actual areas, and there is air flow through the channels between inside and outside of skirt.

(5) Analytical results in case of the emissivity $\varepsilon_{p.v}$=0.95 for outer surface of pressure vessel is between the total heat input and heat transferred to the cooling panel in the vacuum and helium gas conditions.

(6) The analytical results of ratios of thermal radiation to total heat transferred to the cooling panel in case of $\varepsilon_{p.v}$=0.95 are 71.0 and 74.4% for vacuum and helium gas conditions, respectively.

For the benchmark problems of IAEA CRP-3 on GCR afterheat removal in 1995, the experimental data of the case of high temperature condition of pressure vessel (max. 420℃) and of the case of the pressure vessel with stand pipes were selected. And the experimental data of the air cooling panel and the heat pipe cooling panel are also required for the benchmark problems. The further studys of cooling panel tests and development of analytical code will be developed under the international corporation of IAEA CRP-3 on GCR after removal.

ACKNOWLEDGEMENT

The authors would like to thank to Mr. Y. Miyamoto for his helpful suggestions and comments.

REFERENCE

(1) S. Takada, et. al.,"Thermal Analysis Code for Test of Passive Cooling System by Helium Engineering Demonstration Loop (HENDEL) In-core Structure Test Section (T_2) -THANPACST2-", JAERI-Data/Code 95-005(1995).

(2) ASME SECTION Ⅲ, DIVISION 1-APPENDICES, Table Ⅰ-4.0, 112(1989).

(3) A. Goldsmith, et. al. : Handbook of Thermophysical Properties of Solid, Vol.1～5(1961), Pergamon Press.

(4) Siegel-Howell, "Thermal radiation heat transfer", McGraw-Hill Kogakusha, Ltd., 219-282 (1972).

(5) M. Keyhani et. al., Trans. ASME, 105, 454(1983).

(6) M. Fishenden and O. A. Saunders, "Introduction to Heat Transfer", Clarendon Press., 180(1950).

(7) Y. Shiina, et. al., Trans. JSME, 55, 518 (1989).

ACKNOWLEDGEMENT

The authors would like to thank to Mr. Y. Miyamoto for his helpful suggestions and comments.

REFERENCE

(1) S. Takada, et. al.,"Thermal Analysis Code for Test of Passive Cooling System by Helium Engineering Demonstration Loop (HENDEL) In-core Structure Test Section (T_2) -THANPACST2-", JAERI-Data/Code 95-005(1995).

(2) ASME SECTION Ⅲ, DIVISION 1-APPENDICES, Table Ⅰ-4.0, 112(1989).

(3) A. Goldsmith, et. al. : Handbook of Thermophysical Properties of Solid, Vol.1～5(1961), Pergamon Press.

(4) Siegel-Howell, "Thermal radiation heat transfer", McGraw-Hill Kogakusha, Ltd., 219-282 (1972).

(5) M. Keyhani et. al., Trans. ASME, 105, 454(1983).

(6) M. Fishenden and O. A. Saunders, "Introduction to Heat Transfer", Clarendon Press., 180(1950).

(7) Y. Shiina, et. al., Trans. JSME, 55, 518 (1989).

Table 2.1 Correspondence of tag numbers to measuring items (No.1)

Tag Number	Measuring Items	
A1 ~A30	Temperatures on the outer surface of the shell of the pressure vessel (angle 30°)	[℃]
A31~A41	Temperatures on the outer surface of the upper head of the pressure vessel (30°)	[℃]
A42~A46	Temperatures on the outer surface of the lower head of the pressure vessel (30°)	[℃]
A47~A50	Temperatures on the surface of the leg (0°)	[℃]
B1 ~B14	Temperatures on the outer surface of the shell of the pressure vessel (120°)	[℃]
B15~B20	Temperatures on the outer surface of the upper head of the pressure vessel (120°)	[℃]
B21~B22	Temperatures on the outer surface of the lower head of the pressure vessel (120°)	[℃]
B23	Temperature on the surface of the leg (90°)	[℃]
C1 ~C19	Temperatures on the outer surface of the shell of the pressure vessel (210°)	[℃]
C20~C26	Temperatures on the outer surface of the upper head of the pressure vessel (210°)	[℃]
C27~C28	Temperatures on the outer surface of the lower head of the pressure vessel (210°)	[℃]
C29	Temperature on the surface of the leg (180°)	[℃]
D1 ~D20	Temperatures on the outer surface of the shell of the pressure vessel (300°)	[℃]
D21~D28	Temperatures on the outer surface of the upper head of the pressure vessel (300°)	[℃]
D29~D32	Temperatures on the outer surface of the lower head of the pressure vessel (300°)	[℃]
D33	Temperature on the surface of the leg (270°)	[℃]
E1 ~E3	Temperatures on the surface of the top heater segment (No.1)	[℃]
E4 ~E19	Temperatures on the surfaces of the middle heater segments (No.2~No.5)	[℃]
E20~E22	Temperatures on the surface of the bottom heater segment (No.6)	[℃]
E23	Temperatures on the inner surface of the pressure vessel (30°)	[℃]
E24	Temperatures on the inner surface of the pressure vessel (210°)	[℃]
E25	Temperatures on the inner surface of the pressure vessel (300°)	[℃]
E26~E28	Temperatures of helium gas in the pressure vessel	[℃]

Table 2.1 Correspondence of tag numbers to measuring items (No.2)

Tag Number	Measuring Items	
F1 ~F8	Temperatures on the surfaces of the cooling tubes of the side cooling panel	[℃]
F9 ~F10	Temperatures on the surfaces of the cooling tubes of the upper cooling panel	[℃]
F11~F12	Temperatures on the surfaces of the cooling tubes of the lower cooling panel	[℃]
F13~F22	Temperatures on the inner surface of the side wall of the insulator	[℃]
F23	Temperature on the inner surface of the upper wall of the insulator	[℃]
F24	Temperature on the inner surface of the lower wall of the insulator	[℃]
F25~F27	Temperatures on the outer surface of the side wall of the insulator	[℃]
F28	Temperature on the outer surface of the upper wall of the insulator	[℃]
F29	Temperature on the outer surface of the lower wall of the insulator	[℃]
K1 ~K9	Temperatures on the outer surface of the shell of the pressure vessel	[℃]
K10	Temperature on the surface of the upper head of the pressure vessel	[℃]
W1	Inlet temperature of cooling water	[℃]
W2	Outlet temperature of cooling water (Lower cooling panel No.1)	[℃]
W3	Outlet temperature of cooling water (Lower cooling panel No.2)	[℃]
W4	Outlet temperature of cooling water (Side cooling panel No.1)	[℃]
W5	Outlet temperature of cooling water (Side cooling panel No.2)	[℃]
W6	Outlet temperature of cooling water (Upper cooling panel No.1)	[℃]
W7	Outlet temperature of cooling water (Upper cooling panel No.2)	[℃]

Diameter of thermocouples:	A, B, C, D, F	;	ϕ1.0mm
	E	;	ϕ1.6mm
	K	;	ϕ0.5mm
Diameter of resistance bulbs:	W	;	ϕ3.2mm

Table 2.1 Correspondence of tag numbers to measuring items (No.3)

Tag Number	Measuring Items	
PD1	Working fluid gas pressure in the pressure vessel	[kgf/cm^{2}G]
FD1	Flowrate of cooling water (Lower cooling panel No.1)	[l/h]
FD2	Flowrate of cooling water (Lower cooling panel No.2)	[l/h]
FD3	Flowrate of cooling water (Side cooling panel No.1)	[l/h]
FD4	Flowrate of cooling water (Side cooling panel No.2)	[l/h]
FD5	Flowrate of cooling water (Upper cooling panel No.1)	[l/h]
FD6	Flowrate of cooling water (Upper cooling panel No.2)	[l/h]
PW1	Output power of the heater segment No.1	[kW]
PW2	Output power of the heater segment No.2	[kW]
PW3	Output power of the heater segment No.3	[kW]
PW4	Output power of the heater segment No.4	[kW]
PW5	Output power of the heater segment No.5	[kW]
PW6	Output power of the heater segment No.6	[kW]
WP1	Enthalpy difference of water in the lower cooling panel No.1	[kW]
WP2	Enthalpy difference of water in the lower cooling panel No.2	[kW]
WP3	Enthalpy difference of water in the side cooling panel No.1	[kW]
WP4	Enthalpy difference of water in the side cooling panel No.2	[kW]
WP5	Enthalpy difference of water in the upper cooling panel No.1	[kW]
WP6	Enthalpy difference of water in the upper cooling panel No.2	[kW]
THP	Total output power of the heater	[kW]
TWP	Total enthalpy difference of the cooling water	[kW]
HLS	Total heat loss (THP–TWP)	[kW]
TFL	Total flowrate of cooling water	[l/h]

Table 2.2 Conductivities of materials [2]

Materials \Temperature T[K]	300	400	500	600	800	1000
Stainless steel (SUS304)						
・Pressure vessel	14.9	16.7	18.3	19.7	22.6	25.4
・Thermocouple holder						
・Heater support						
・Heater support plate						
Carbon steel (C-Mn-Si)						
・Cooling tubes	41.0	42.2	41.5	39.7	35.0	27.8
Carbon steel (Plain Carbon)						
・Legs	60.6	56.8	52.7	48.0	39.3	30.1
・Skirt						
Ceramics (Al_2O_3)*	36.0	–	20.2	–	10.4	–
・Heater block						

Unit: [W/mK]

* "Handbook of heat transfer engineering", Vol. 4, 320(1986), JSME.

Table 2.3 Emissivities of materials [3]

Components ＼ Temperature	[℃]	149	260	538	816	
	T[K]	422	533	811	1089	Correlation function
Pressure vessel						
Stainless steel(SUS304)						
Polished		0.07	0.08	0.10	–	$0.0385+7.612\times10^{-5}T$
Oxidazed		0.79	0.79	0.79	–	0.79
Electric heater						
Nichrome Polished		0.66	0.67	0.71	–	$0.603+1.315\times10^{-4}T$
Oxidazed		0.96	0.97	0.98	–	$0.941+4.844\times10^{-5}T$
Ceramics (Al_2O_3)		0.93	0.93	0.67	0.44	0.93 (T<533[K])
						$1.395-8.813\times10^{-4}T$ (T>533[K])

Unit: [-]

Table 2.4 Experimental results of emissivities

Heat flux [kW/m^2]	Temperature [℃]		Emissivities		
	Heater	Pressure vessel	ε	ε_1 (Heater)	ε_2 (Pressure vessel)
1.702	246.5	110.8	0.59	0.65	0.79
2.568	297.1	143.5	0.60	0.66	0.79
4.269	346.3	176.5	0.71	0.80	0.79
5.927	396.3	213.0	0.72	0.81	0.79
7.863	446.5	249.5	0.72	0.81	0.79
10.36	495.6	283.6	0.72	0.82	0.79

Table 3.1 Experimental data of the vacuum condition

(A01)	~~20.0~~	(B01)	93.4	(D01)	94.0	(E01)	298.4	(F01)	25.2
(A02)	104.7	(B02)	106.4	(D02)	104.4	(E02)	294.8	(F02)	24.8
(A03)	105.3	(B03)	105.0	(D03)	105.3	(E03)	270.6	(F03)	24.2
(A04)	106.2	(B04)	106.4	(D04)	105.6	(E04)	294.9	(F04)	24.3
(A05)	122.8	(B05)	125.0	(D05)	122.2	(E05)	298.4	(F05)	23.4
(A06)	127.2	(B06)	127.7	(D06)	128.9	(E06)	289.3	(F06)	23.6
(A07)	130.5	(B07)	131.8	(D07)	131.5	(E07)	~~18.6~~	(F07)	24.2
(A08)	134.9	(B08)	130.5	(D08)	131.8	(E08)	298.6	(F08)	23.8
(A09)	131.4	(B09)	131.8	(D09)	129.9	(E09)	296.9	(F09)	26.2
(A10)	136.0	(B10)	135.8	(D10)	136.0	(E10)	296.9	(F10)	24.7
(A11)	130.8	(B11)	139.0	(D11)	143.4	(E11)	297.6	(F11)	24.2
(A12)	138.4	(B12)	138.7	(D12)	~~2087.6~~	(E12)	296.5	(F12)	25.0
(A13)	144.8	(B13)	142.6	(D13)	~~2000.1~~	(E13)	301.0	(F13)	30.8
(A14)	~~20.6~~	(B14)	135.5	(D14)	142.5	(E14)	298.7	(F14)	45.1
(A15)	145.8	(B15)	117.0	(D15)	142.7	(E15)	282.0	(F15)	48.2
(A16)	143.2	(B16)	117.0	(D16)	145.0	(E16)	293.8	(F16)	44.4
(A17)	138.8	(B17)	119.1	(D17)	144.8	(E17)	293.3	(F17)	45.5
(A18)	141.2	(B18)	112.0	(D18)	135.9	(E18)	293.7	(F18)	48.3
(A19)	142.1	(B19)	108.6	(D19)	118.8	(E19)	297.9	(F19)	45.0
(A20)	141.5	(B20)	99.8	(D20)	98.3	(E20)	296.8	(F20)	45.6
(A21)	141.9	(B21)	132.8	(D21)	115.5	(E21)	293.1	(F21)	50.3
(A22)	143.4	(B22)	108.9	(D22)	114.9	(E22)	272.1	(F22)	46.3
(A23)	140.0	(B23)	36.1	(D23)	117.7	(E23)	150.6	(F23)	52.7
(A24)	145.2	(C01)	93.9	(D24)	115.4	(E24)	157.8	(F24)	35.5
(A25)	146.3	(C02)	106.5	(D25)	112.6	(E25)	154.3	(F25)	22.2
(A26)	138.7	(C03)	105.3	(D26)	109.4	(E26)	244.0	(F26)	25.7
(A27)	135.3	(C04)	105.5	(D27)	108.3	(E27)	233.0	(F27)	22.1
(A28)	125.8	(C05)	122.5	(D28)	102.0	(E28)	264.9	(F28)	24.5
(A29)	119.9	(C06)	126.0	(D29)	125.3	(K01)	141.1	(F29)	23.7
(A30)	103.8	(C07)	131.6	(D30)	131.9	(K02)	147.7		
(A31)	116.8	(C08)	128.7	(D31)	126.4	(K03)	145.8		
(A32)	115.9	(C09)	129.0	(D32)	112.2	(K04)	144.4		
(A33)	116.0	(C10)	137.5	(D33)	35.4	(K05)	~~21.2~~		
(A34)	119.5	(C11)	140.4	(W01)	21.416	(K06)	145.8		
(A35)	119.8	(C12)	143.6	(W02)	22.056	(K07)	143.5		
(A36)	116.9	(C13)	145.5	(W03)	22.293	(K08)	143.2		
(A37)	113.5	(C14)	145.6	(W04)	22.838	(K09)	144.1		
(A38)	110.0	(C15)	148.8	(W05)	22.855	(K10)	113.2		
(A39)	107.8	(C16)	146.9	(W06)	21.827	(PD1)	-.937		
(A40)	100.1	(C17)	136.8	(W07)	21.995	(FD1)	90.8		
(A41)	92.2	(C18)	119.8	(WP1)	.068	(FD2)	80.1		
(A42)	~~21.6~~	(C19)	95.3	(WP2)	.082	(FD3)	2967.7		
(A43)	130.3	(C20)	116.7	(WP3)	4.907	(FD4)	2998.7		
(A44)	134.7	(C21)	116.3	(WP4)	5.018	(FD5)	1008.0		
(A45)	127.1	(C22)	116.1	(WP5)	.482	(FD6)	993.6		
(A46)	119.1	(C23)	118.4	(WP6)	.669	(PW1)	1.010		
(A47)	52.8	(C24)	117.3	(TWP)	11.224	(PW2)	2.306		
(A48)	43.8	(C25)	113.3	(THP)	13.140	(PW3)	2.636		
(A49)	38.1	(C26)	102.0	(HLS)	1.916	(PW4)	2.460		
(A50)	34.0	(C27)	129.4	(TFL)	8138.9	(PW5)	3.763		
		(C28)	108.8			(PW6)	.964		
		(C29)	36.9						

Deletion lines mean the measurement values by broken thermo-couples.

Table 3.2 Experimental data of the helium gas condition

(A01)	~~27.0~~	(B01)	156.1	(D01)	157.4	(E01)	301.1	(F01)	22.9
(A02)	176.6	(B02)	178.0	(D02)	176.8	(E02)	298.4	(F02)	22.5
(A03)	177.6	(B03)	177.4	(D03)	178.9	(E03)	291.4	(F03)	22.0
(A04)	176.8	(B04)	178.6	(D04)	178.0	(E04)	301.3	(F04)	21.2
(A05)	187.5	(B05)	191.3	(D05)	188.7	(E05)	302.8	(F05)	19.7
(A06)	190.8	(B06)	190.2	(D06)	191.6	(E06)	299.0	(F06)	20.0
(A07)	189.1	(B07)	189.9	(D07)	190.1	(E07)	~~10.5~~	(F07)	20.6
(A08)	195.7	(B08)	190.6	(D08)	192.5	(E08)	303.8	(F08)	20.1
(A09)	191.3	(B09)	190.2	(D09)	190.4	(E09)	297.8	(F09)	26.8
(A10)	196.6	(B10)	194.1	(D10)	191.0	(E10)	300.1	(F10)	22.6
(A11)	190.6	(B11)	194.3	(D11)	196.2	(E11)	302.3	(F11)	19.4
(A12)	191.5	(B12)	192.2	(D12)	~~8896.0~~	(E12)	305.1	(F12)	19.2
(A13)	195.5	(B13)	193.6	(D13)	~~9000.0~~	(E13)	312.2	(F13)	32.1
(A14)	~~26.7~~	(B14)	192.8	(D14)	194.4	(E14)	303.9	(F14)	64.0
(A15)	196.7	(B15)	209.3	(D15)	194.0	(E15)	272.3	(F15)	64.4
(A16)	194.6	(B16)	208.3	(D16)	196.1	(E16)	292.9	(F16)	57.5
(A17)	189.3	(B17)	211.2	(D17)	197.1	(E17)	292.5	(F17)	64.8
(A18)	192.0	(B18)	202.0	(D18)	192.3	(E18)	294.1	(F18)	64.4
(A19)	193.6	(B19)	198.9	(D19)	178.5	(E19)	279.5	(F19)	58.7
(A20)	192.6	(B20)	182.3	(D20)	152.1	(E20)	301.0	(F20)	65.3
(A21)	192.9	(B21)	170.0	(D21)	206.5	(E21)	296.7	(F21)	67.7
(A22)	194.0	(B22)	147.4	(D22)	203.0	(E22)	275.9	(F22)	61.1
(A23)	188.9	(B23)	38.9	(D23)	201.2	(E23)	197.1	(F23)	80.3
(A24)	194.8	(C01)	156.8	(D24)	198.5	(E24)	201.0	(F24)	38.5
(A25)	197.4	(C02)	179.5	(D25)	196.7	(E25)	199.7	(F25)	20.5
(A26)	190.8	(C03)	178.1	(D26)	195.0	(E26)	290.4	(F26)	22.9
(A27)	191.1	(C04)	176.8	(D27)	192.8	(E27)	286.8	(F27)	16.8
(A28)	182.8	(C05)	189.7	(D28)	183.6	(E28)	277.3	(F28)	21.2
(A29)	180.0	(C06)	188.9	(D29)	173.9	(K01)	195.6	(F29)	18.5
(A30)	156.0	(C07)	190.2	(D30)	170.1	(K02)	198.3		
(A31)	209.7	(C08)	190.0	(D31)	154.6	(K03)	197.4		
(A32)	207.3	(C09)	190.1	(D32)	149.8	(K04)	195.1		
(A33)	207.1	(C10)	195.7	(D33)	38.1	(K05)	~~28.9~~		
(A34)	208.0	(C11)	195.3	(W01)	14.848	(K06)	196.9		
(A35)	205.8	(C12)	196.8	(W02)	15.845	(K07)	196.5		
(A36)	201.6	(C13)	196.8	(W03)	16.359	(K08)	194.9		
(A37)	198.0	(C14)	196.3	(W04)	17.815	(K09)	195.6		
(A38)	193.6	(C15)	198.7	(W05)	17.793	(K10)	197.2		
(A39)	190.8	(C16)	198.6	(W06)	16.107	(PD1)	6.255		
(A40)	181.6	(C17)	192.9	(W07)	16.229	(FD1)	127.0		
(A41)	159.0	(C18)	180.4	(WP1)	.147	(FD2)	102.6		
(A42)	~~27.0~~	(C19)	150.7	(WP2)	.180	(FD3)	3115.0		
(A43)	180.4	(C20)	208.5	(WP3)	10.749	(FD4)	3108.2		
(A44)	176.6	(C21)	207.1	(WP4)	10.644	(FD5)	1026.3		
(A45)	165.4	(C22)	205.5	(WP5)	1.503	(FD6)	1054.6		
(A46)	158.9	(C23)	202.4	(WP6)	1.694	(PW1)	1.157		
(A47)	68.6	(C24)	198.8	(TWP)	24.919	(PW2)	3.106		
(A48)	51.3	(C25)	194.3	(THP)	28.791	(PW3)	3.524		
(A49)	41.4	(C26)	182.6	(HLS)	3.873	(PW4)	5.096		
(A50)	34.7	(C27)	170.4	(TFL)	8533.8	(PW5)	10.415		
		(C28)	150.6			(PW6)	5.492		
		(C29)	40.0						

Deletion lines mean the measurement values by broken thermo-couples.

Table 4.1 Heat transfer coefficients on components

Region No.	Ra	Nu m	Equation No.
①	4.35×10^{8}	38.0	[4.3]
②	5.65×10^{6}	11.4	[4.3]
③	9.43×10^{7}	63.7	[4.4]
④	2.12×10^{10}	387	[4.4]
⑤	2.66×10^{9}	193	[4.4]
⑥	8.92×10^{7}	19.2	[4.5]
⑦	9.43×10^{7}	26.6	[4.6]
⑧	4.37×10^{8}	39.0	[4.6]
⑨	2.66×10^{9}	61.3	[4.6]

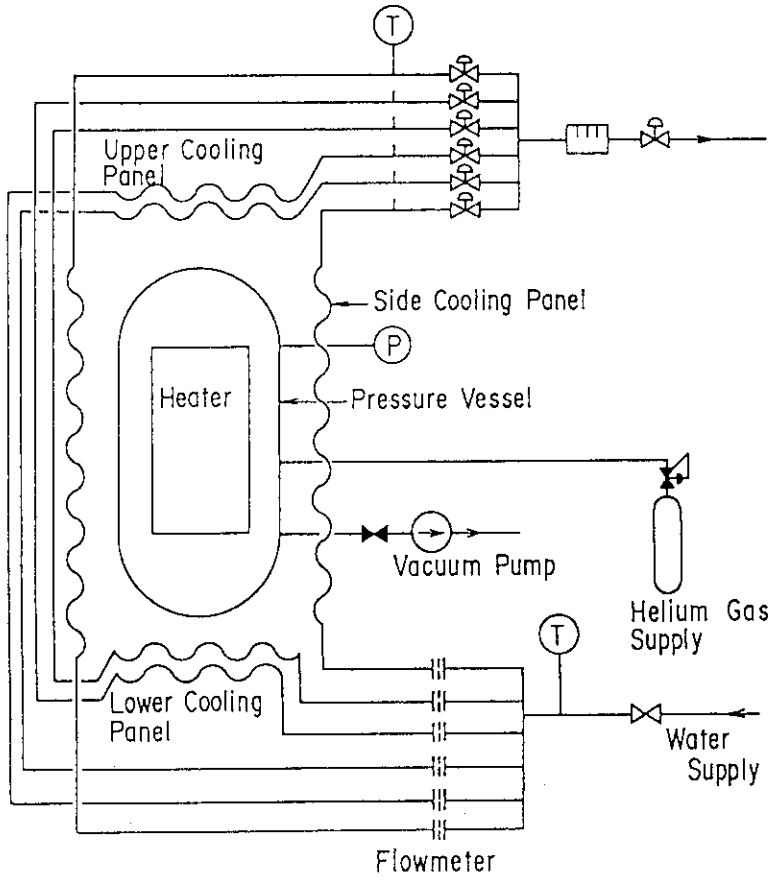

Fig.2.1 Flowsheet of test apparatus

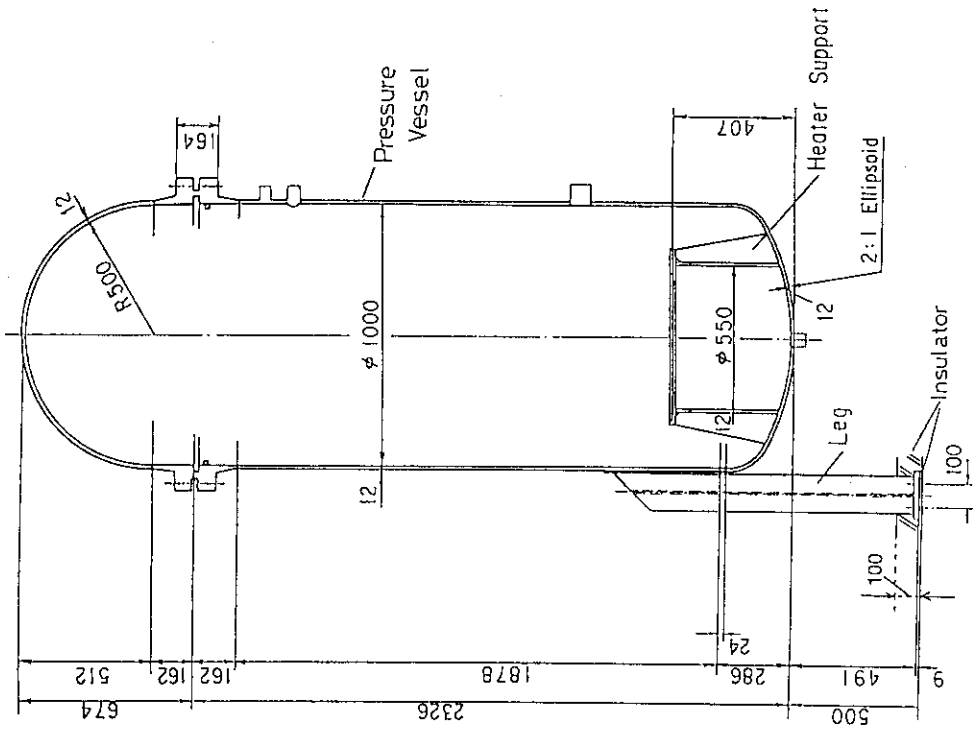

Fig.2.3 Pressure vessel, leg and heater support

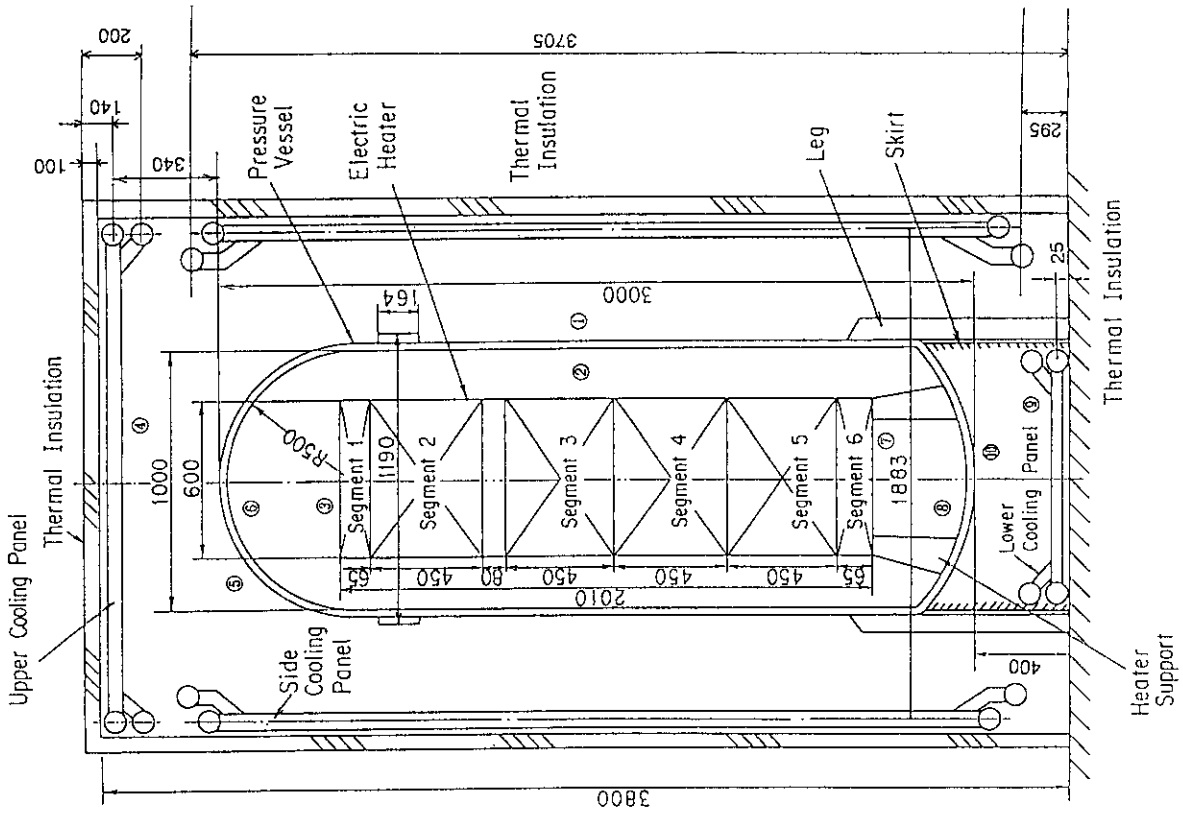

Fig.2.2 Schematic diagram of test apparatus

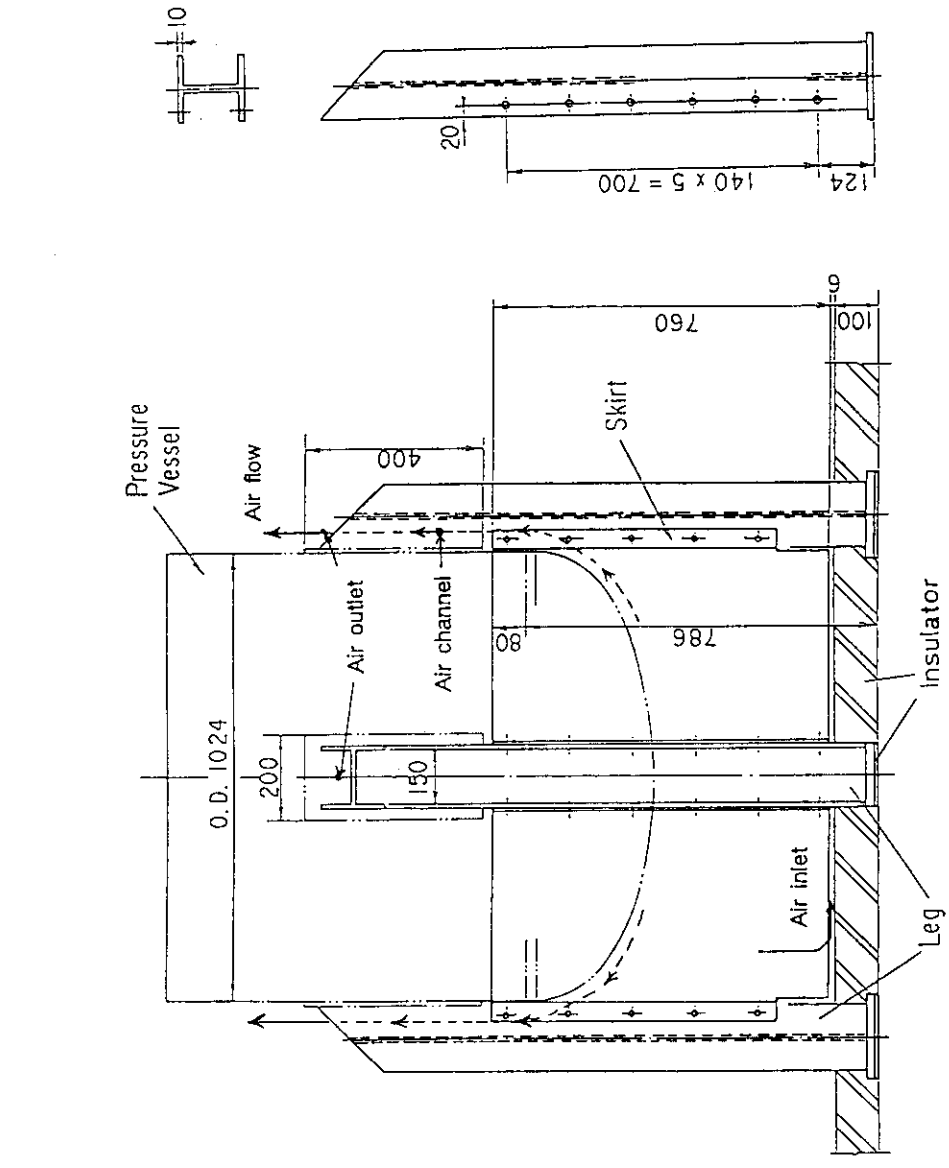

Fig.2.5 Schematic diagrams of leg and skirt

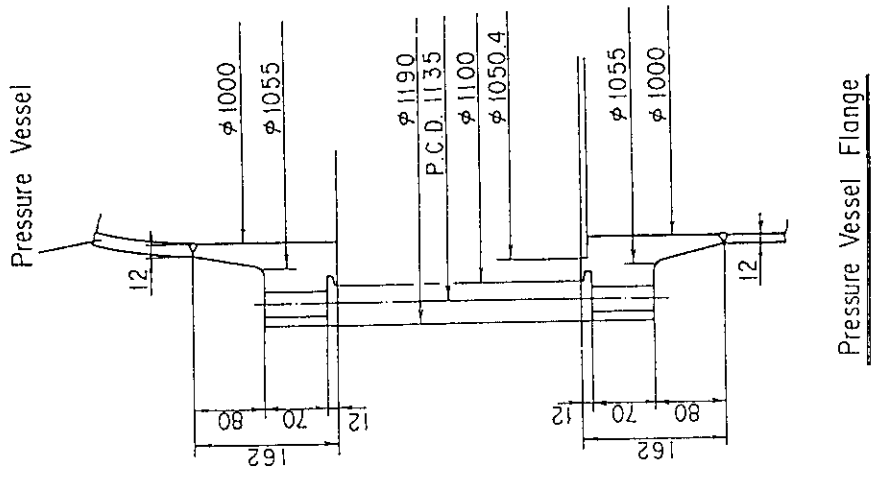

Fig.2.4 Pressure vessel flange

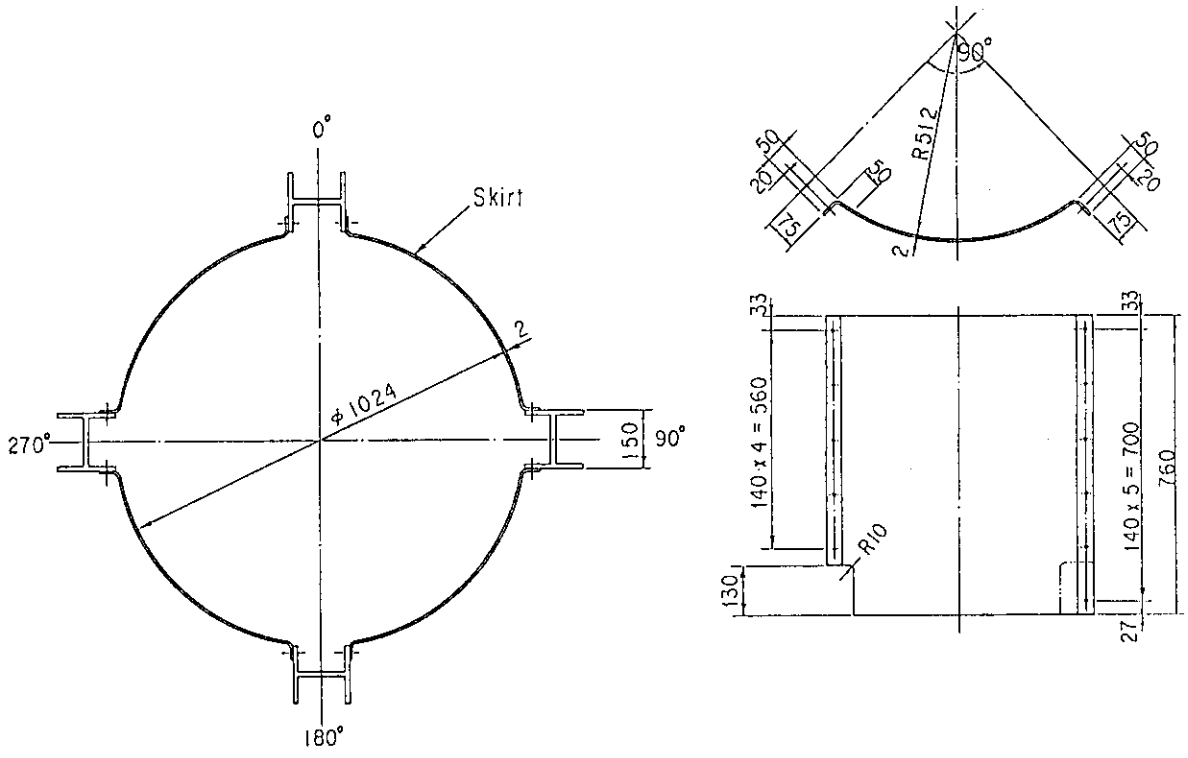

Fig.2.7 Size and detailed configuration of skirt

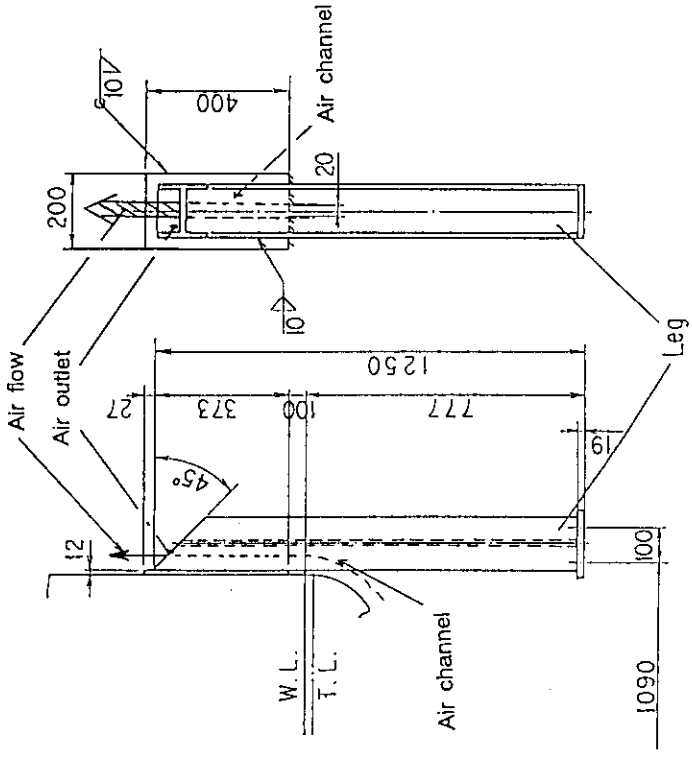

Fig.2.6 Detailed sizes of a leg

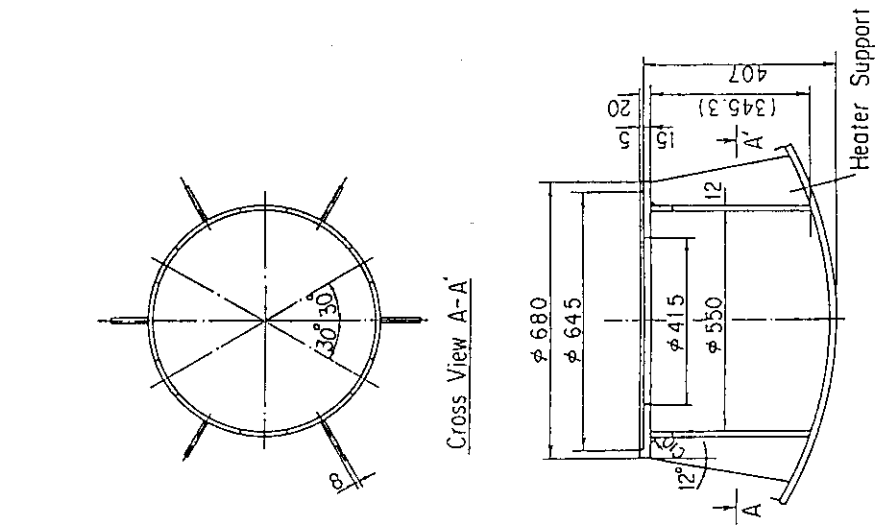

Fig.2.9 Size and detailed configuration of heater support

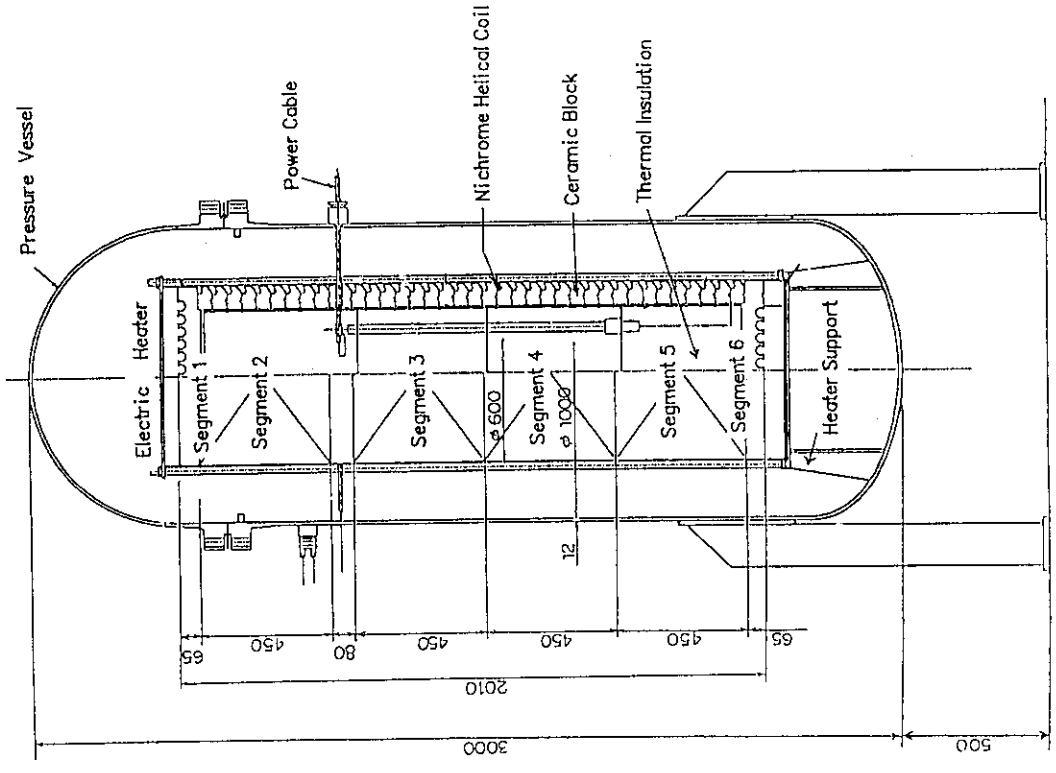

Fig.2.8 Schematic diagram of heater in the pressure vessel

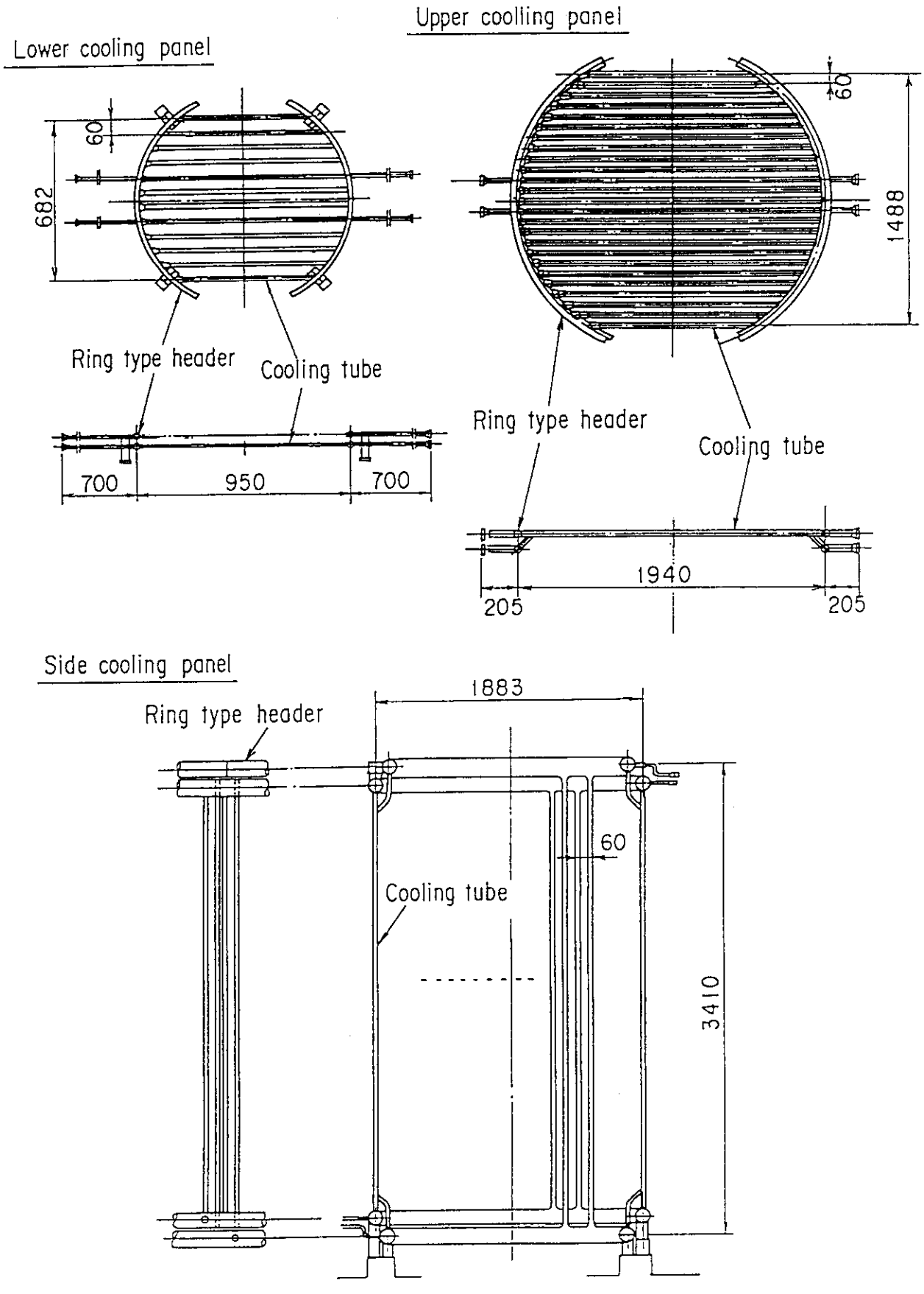

Fig.2.10 Schematic diagrams of lower, upper and side cooling panels

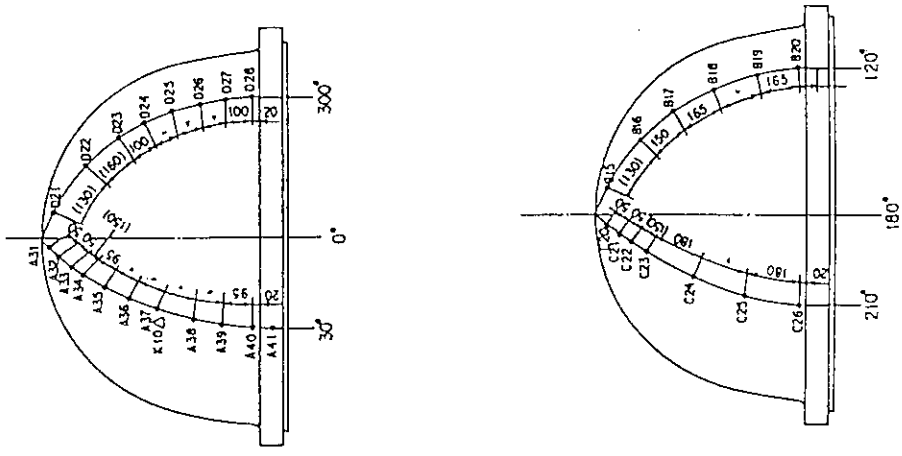

Fig.2.12 Thermocouple positions on the outer surface of the pressure vessel-upper head

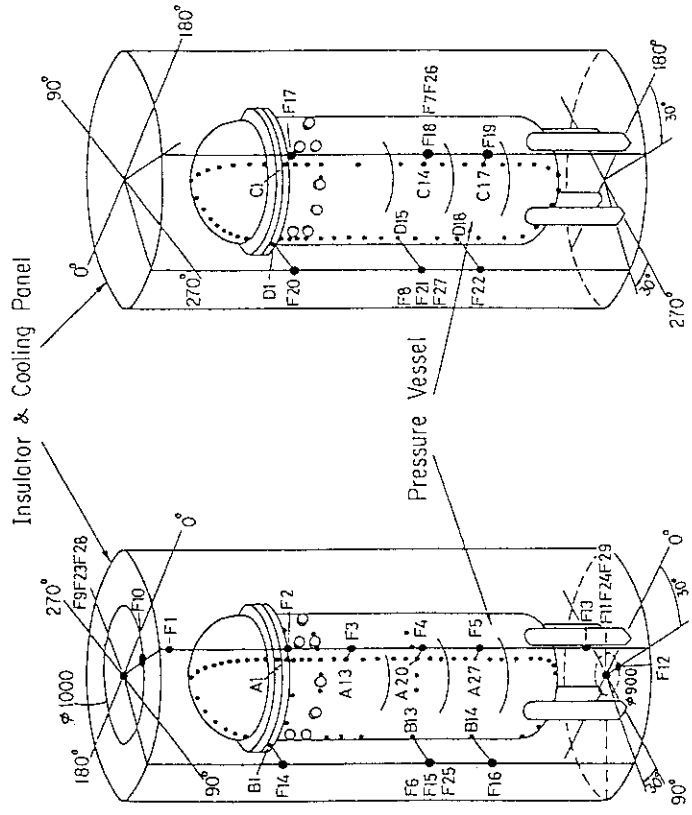

Fig.2.11 Thermocouple positions on the cooling panels, outer surface of the pressure vessel and the thermal insulation surface

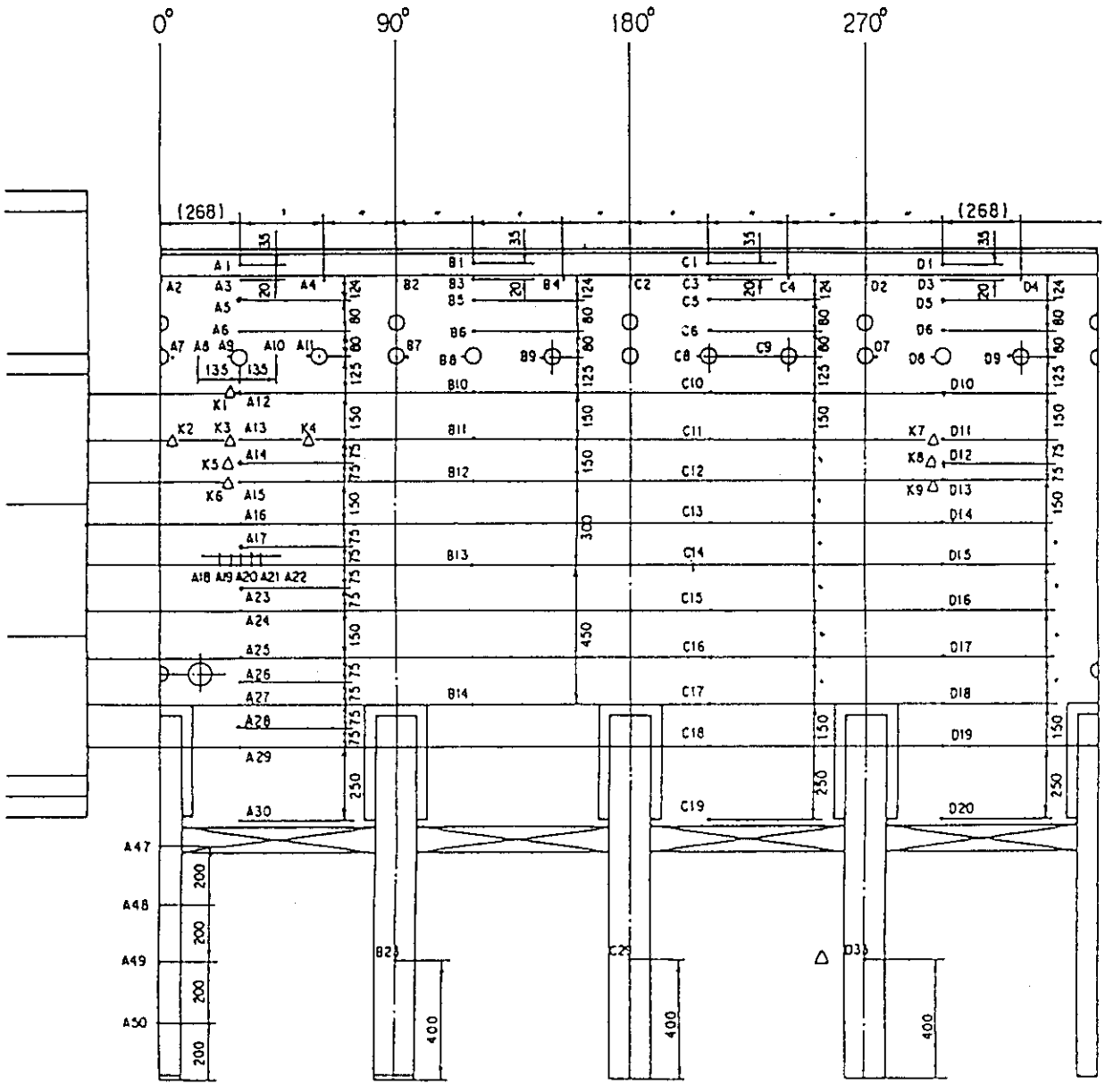

Fig.2.13 Thermocouple positions on the outer surface of the pressure vessel-shell

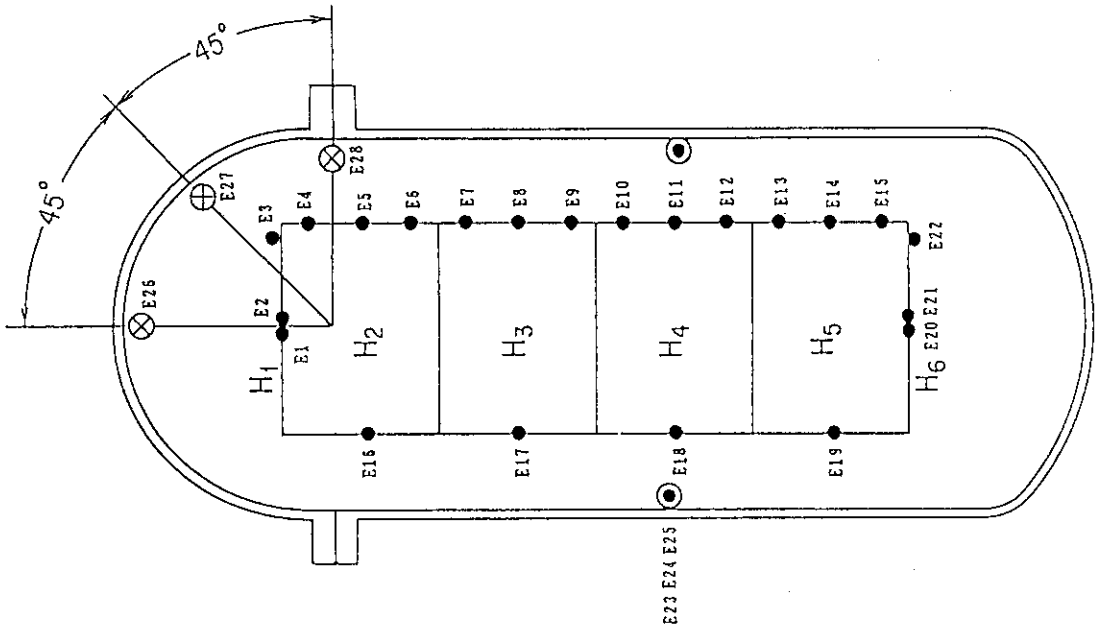

Fig.2.15 Measuring postions of the inner surface temperature of the pressure vessel, gas temperature and heater surface temperature

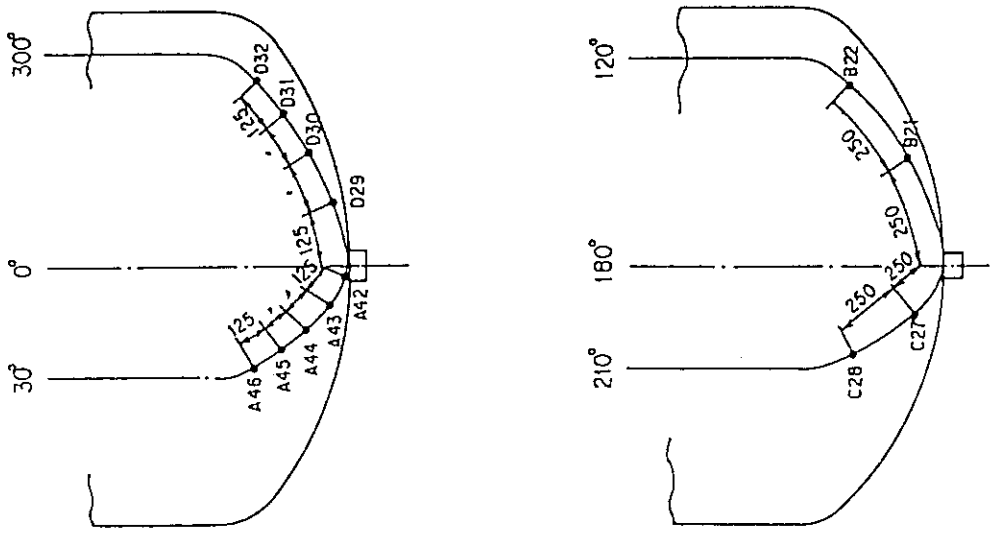

Fig.2.14 Thermocouple positions on the outer surface of the pressure vessel-lower head

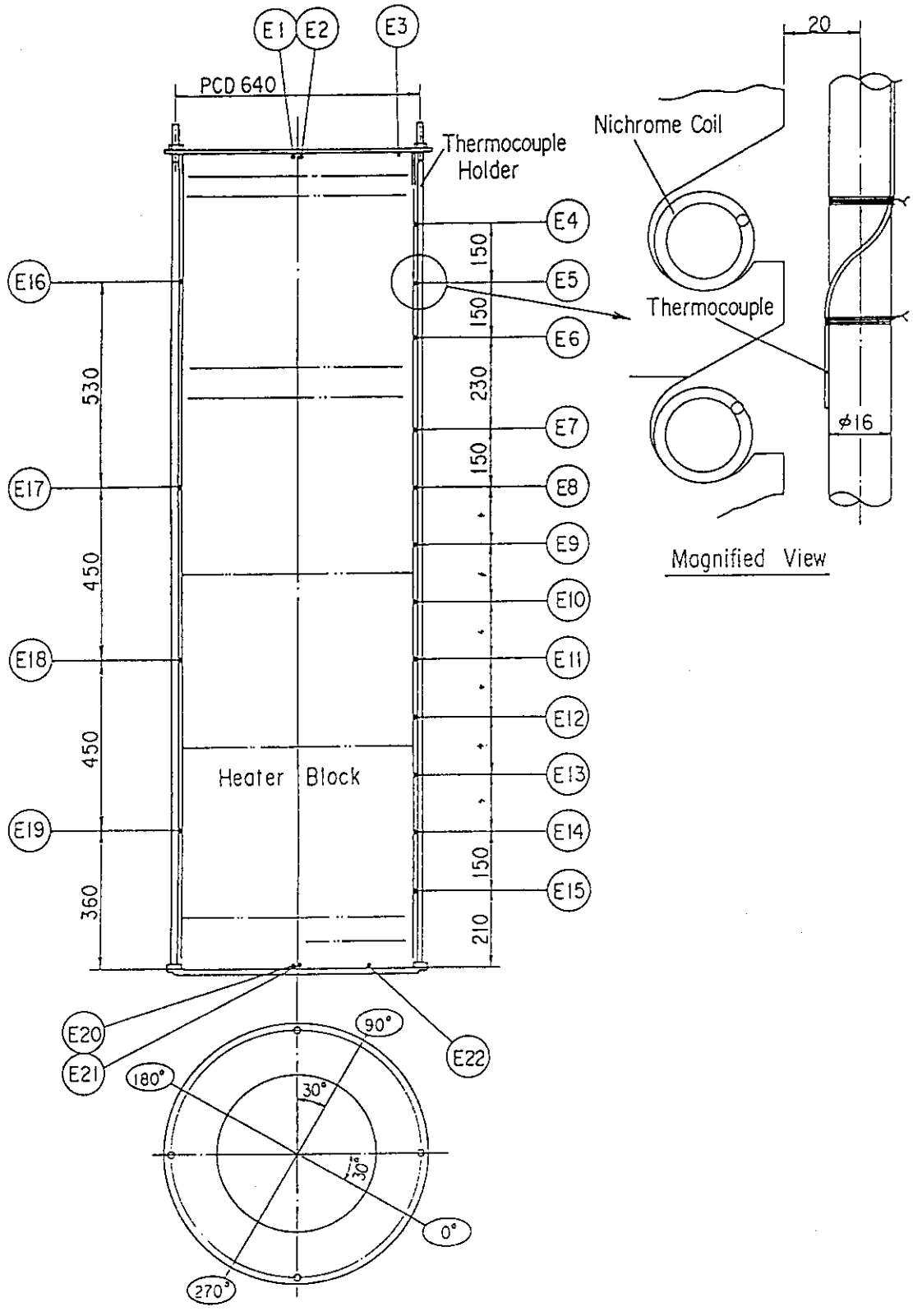

Fig.2.16 Detailed structure of the heater and thermocouple positions on the heater surface

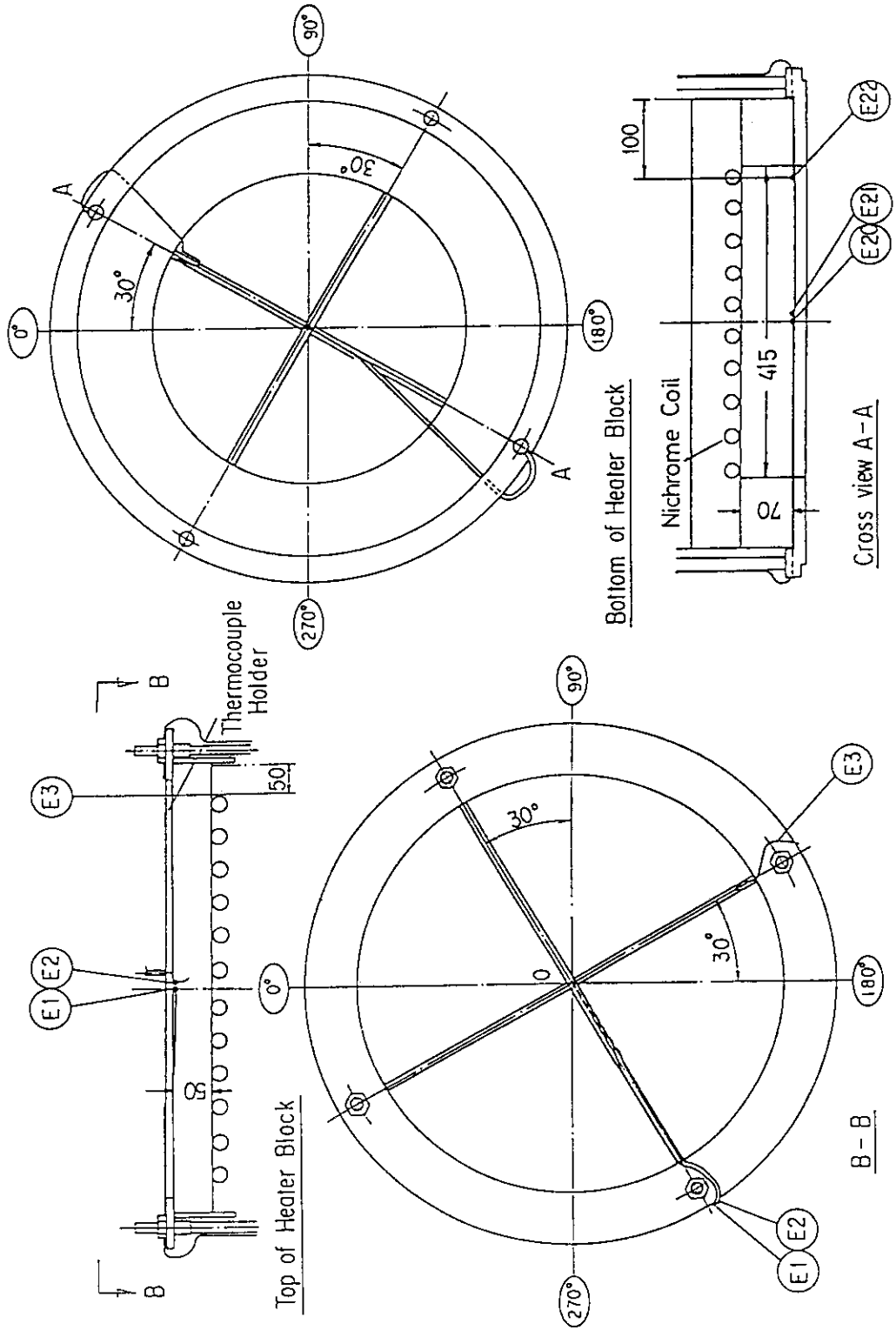

Fig.2.17 Top and bottom of the heater and thermocouple positions on them

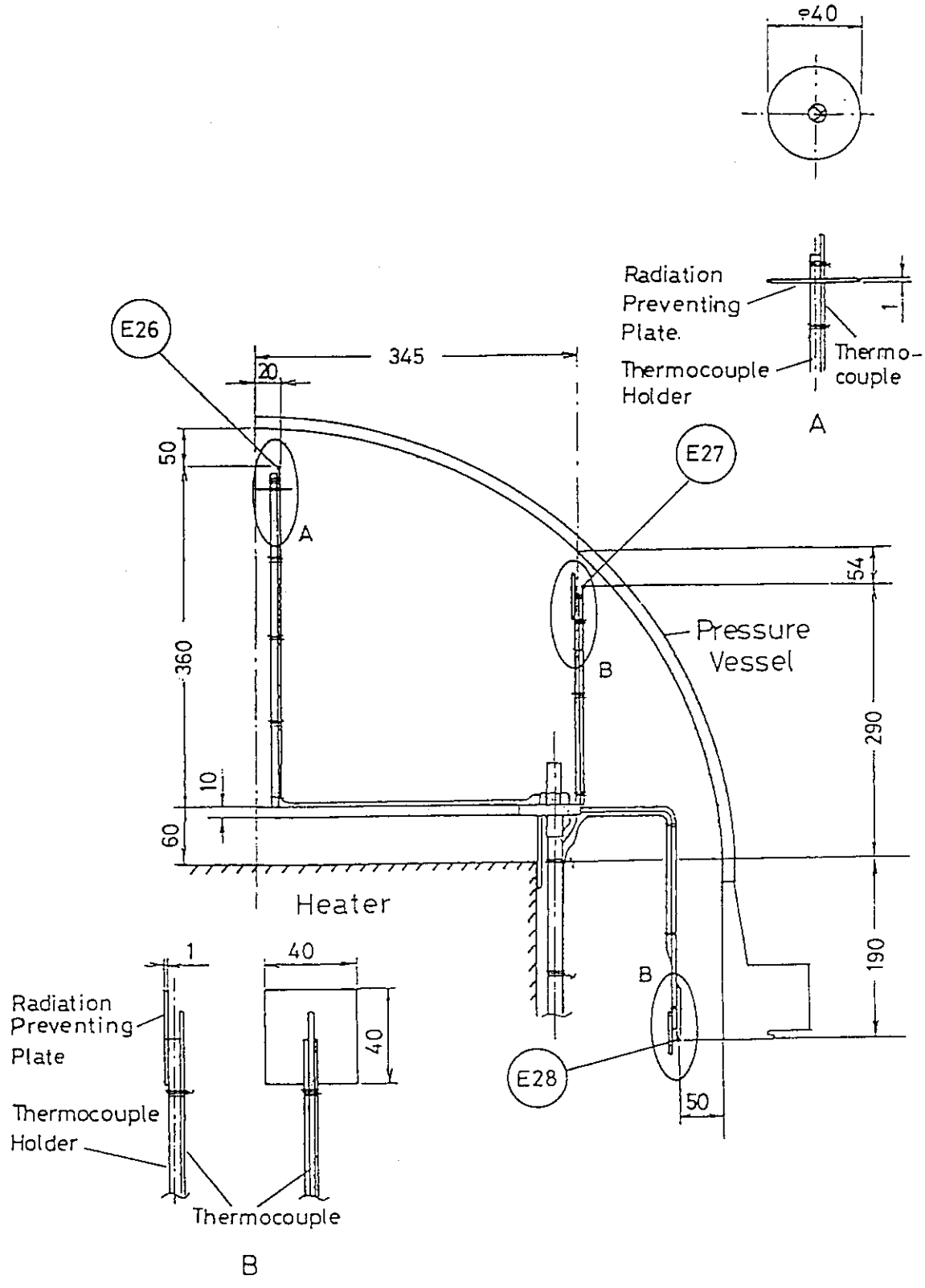

Fig.2.18 Positions of the thermocouples E26, E27 and E28

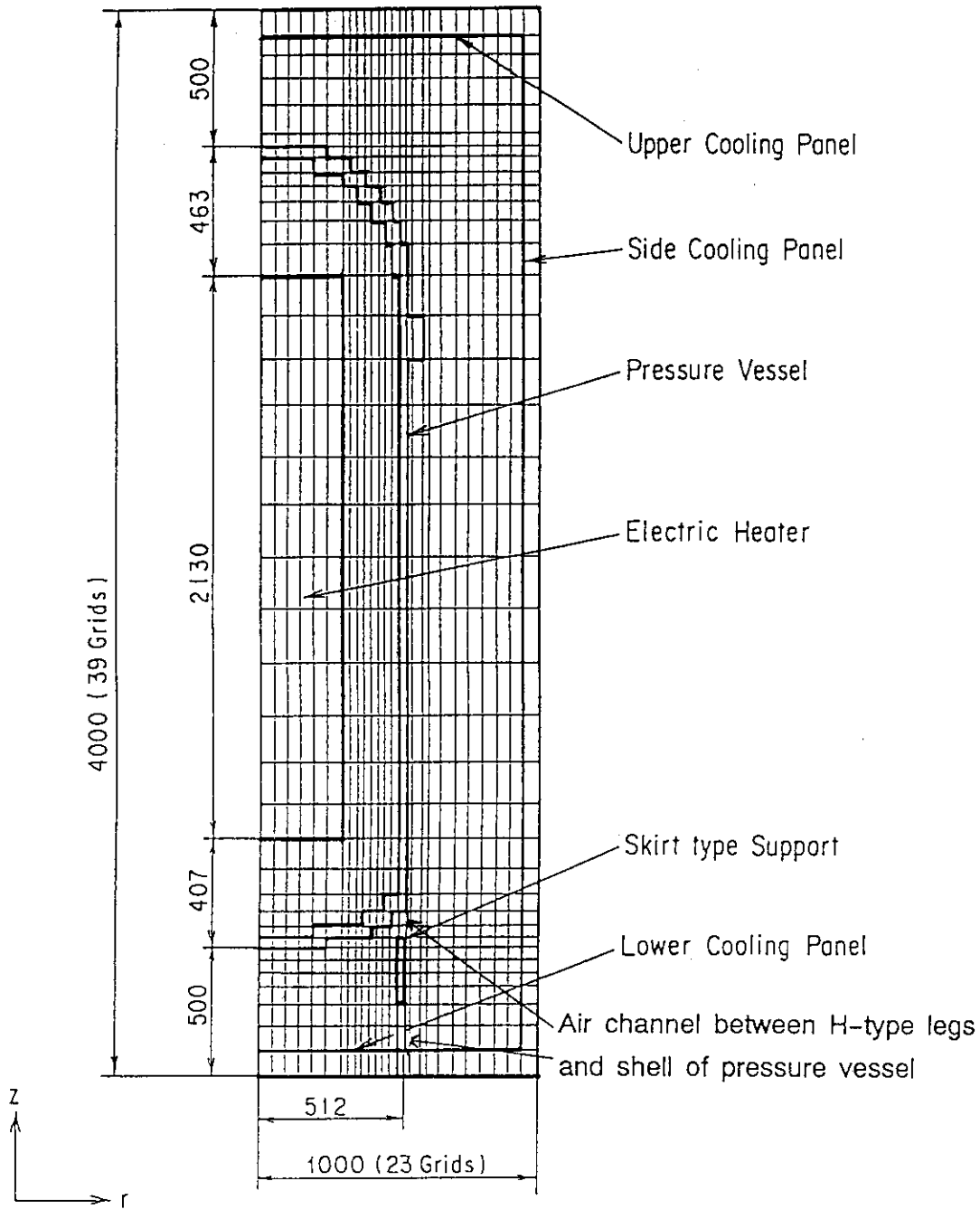

Fig.4.1 Differential scheme of numerical analysis

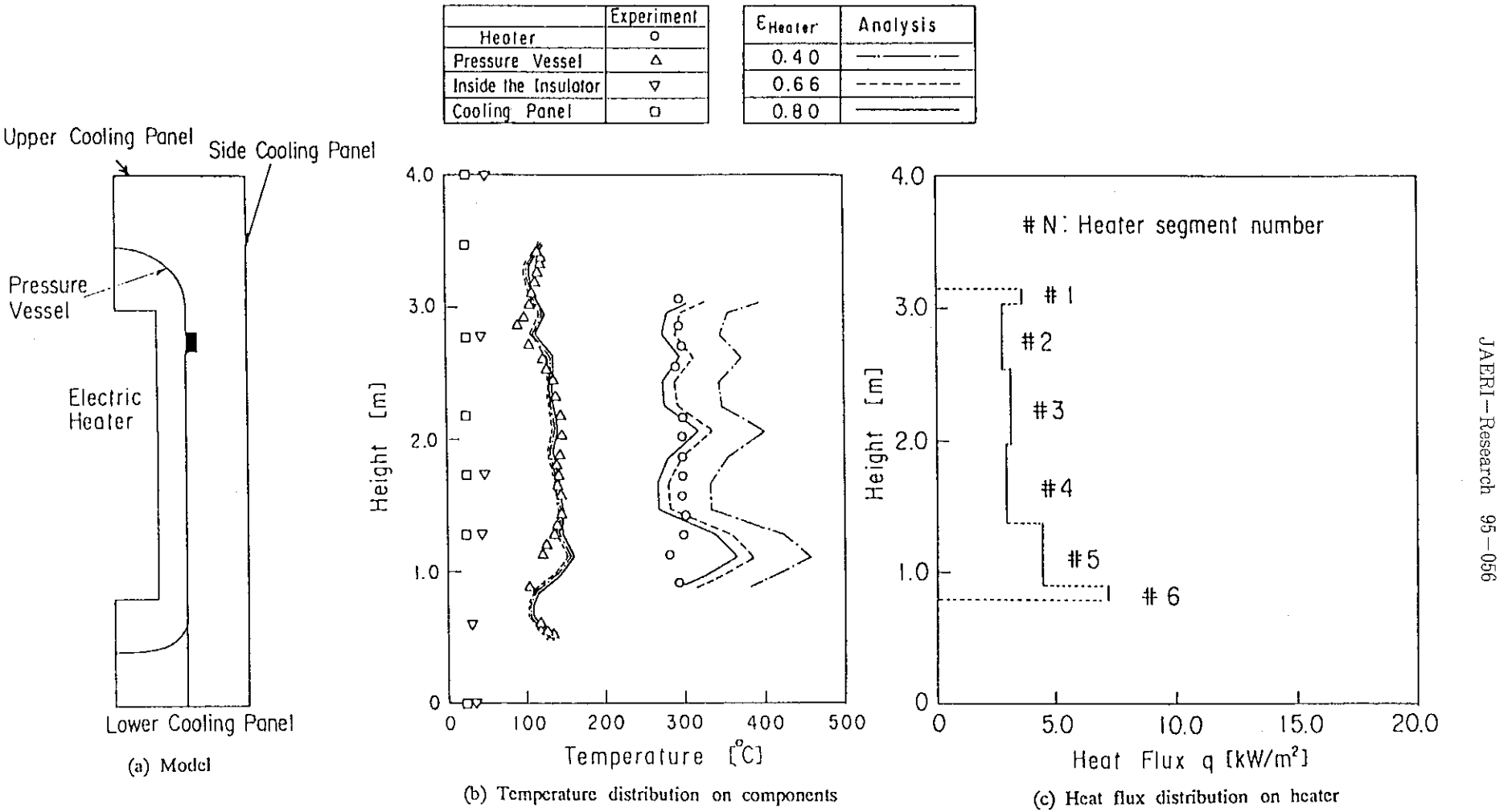

Fig.5.1 Experimental and analytical results
(Vacuum condition)

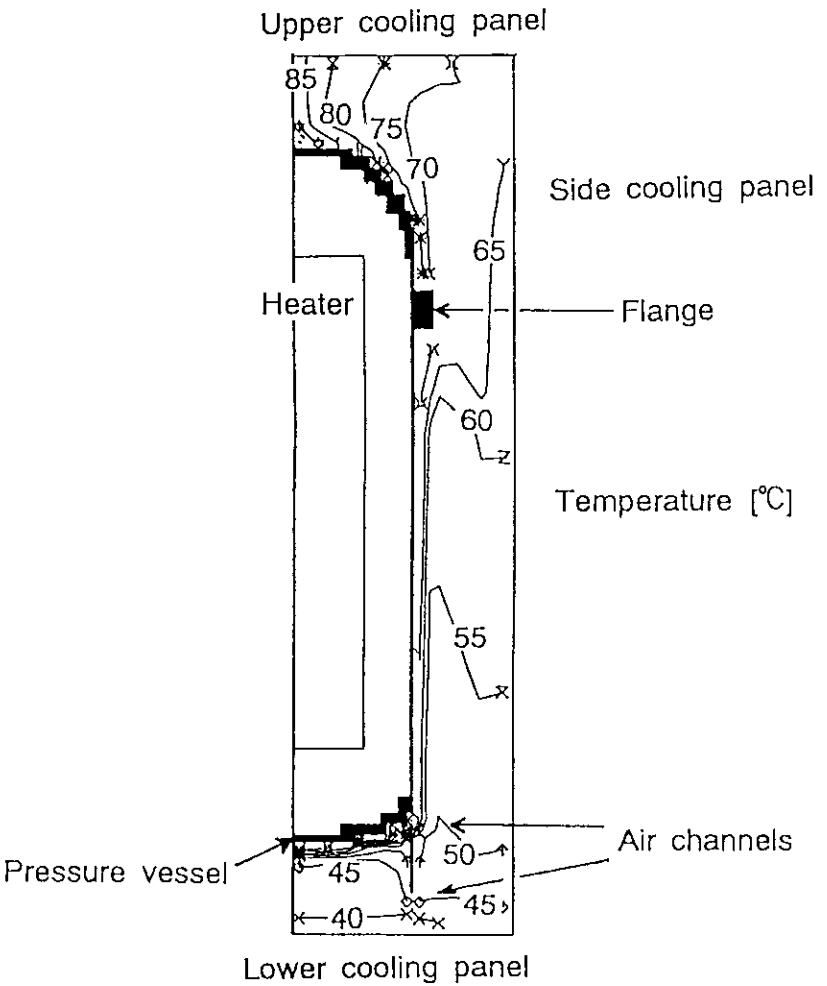

Fig.5.2(a) Analytical results of temperature contour
(Vacuum condition inside the pressure vessel)

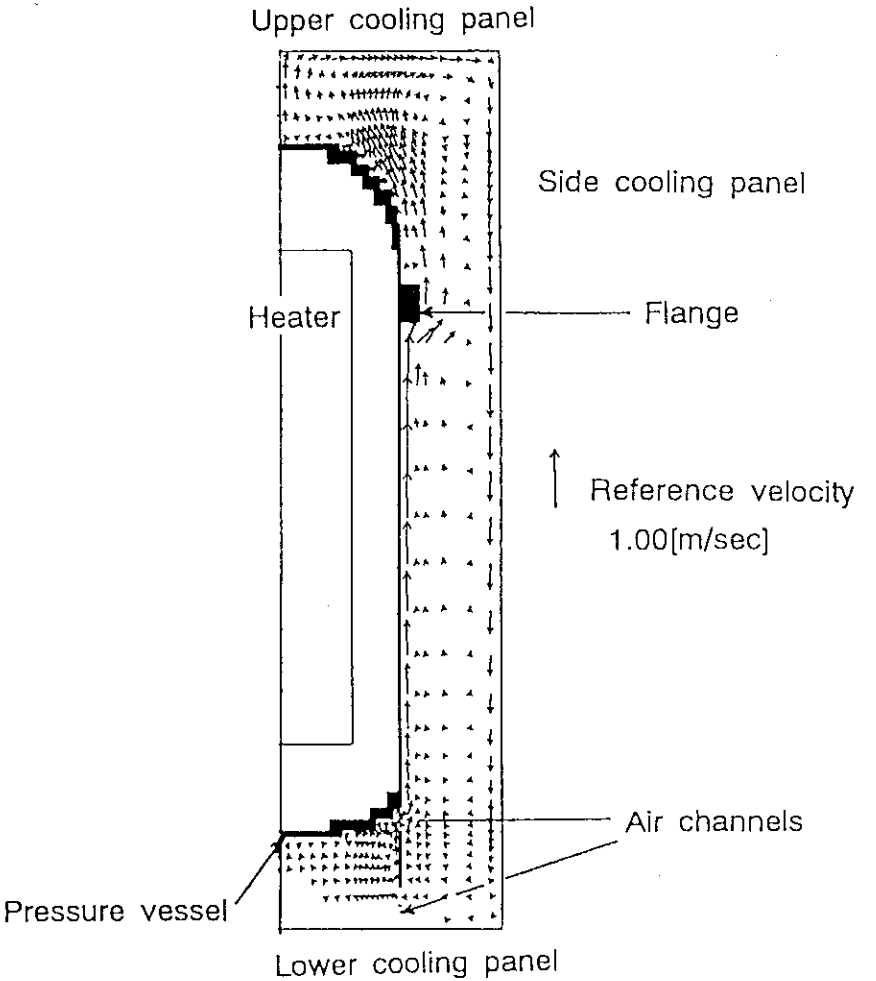

Fig.5.2(b) Analytical results of velocity vector
(Vacuum condition inside the pressure vessel)

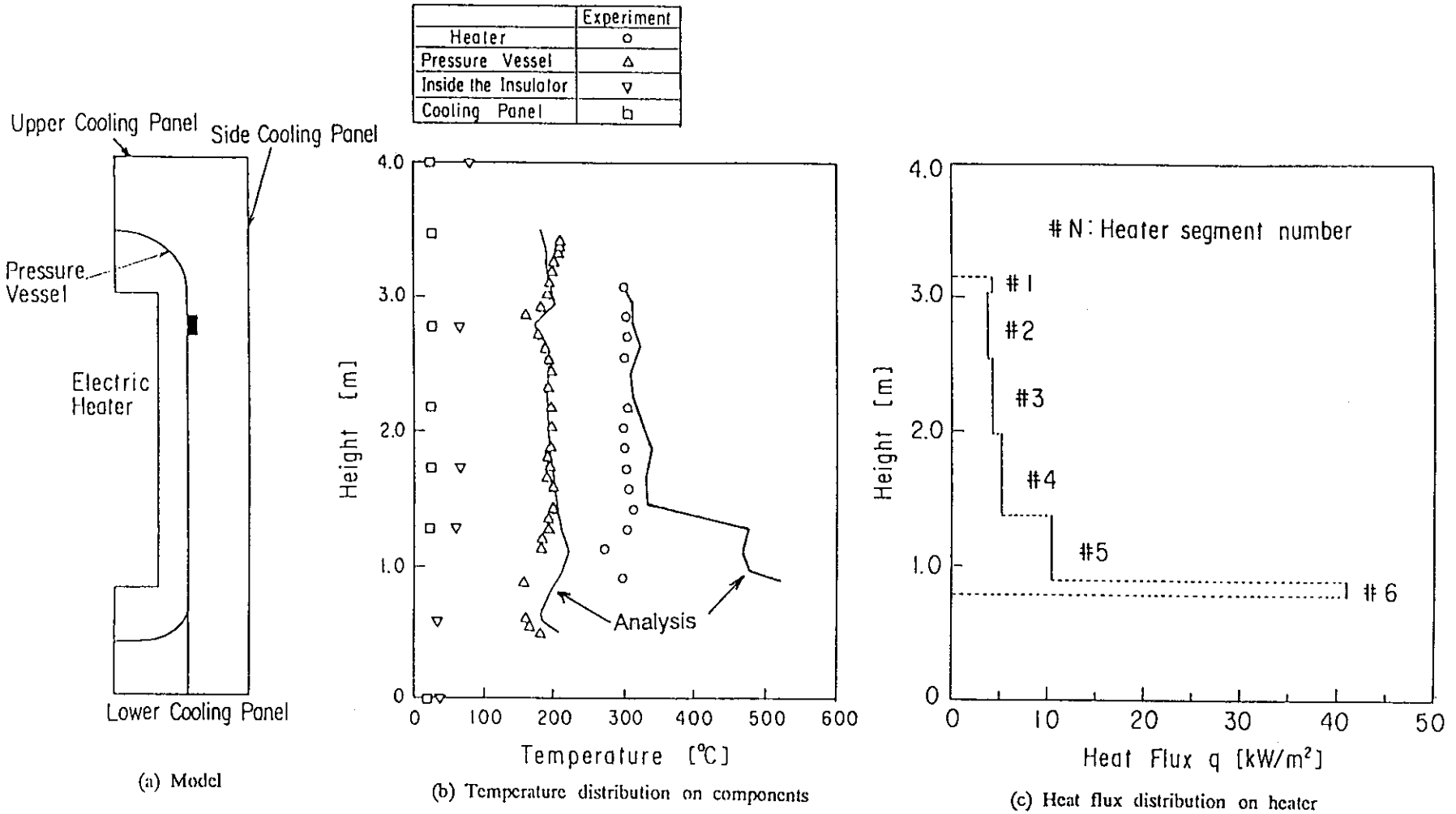

(a) Model

(b) Temperature distribution on components

(c) Heat flux distribution on heater

Fig.5.3 Experimental and analytical results
(Helium gas condition)

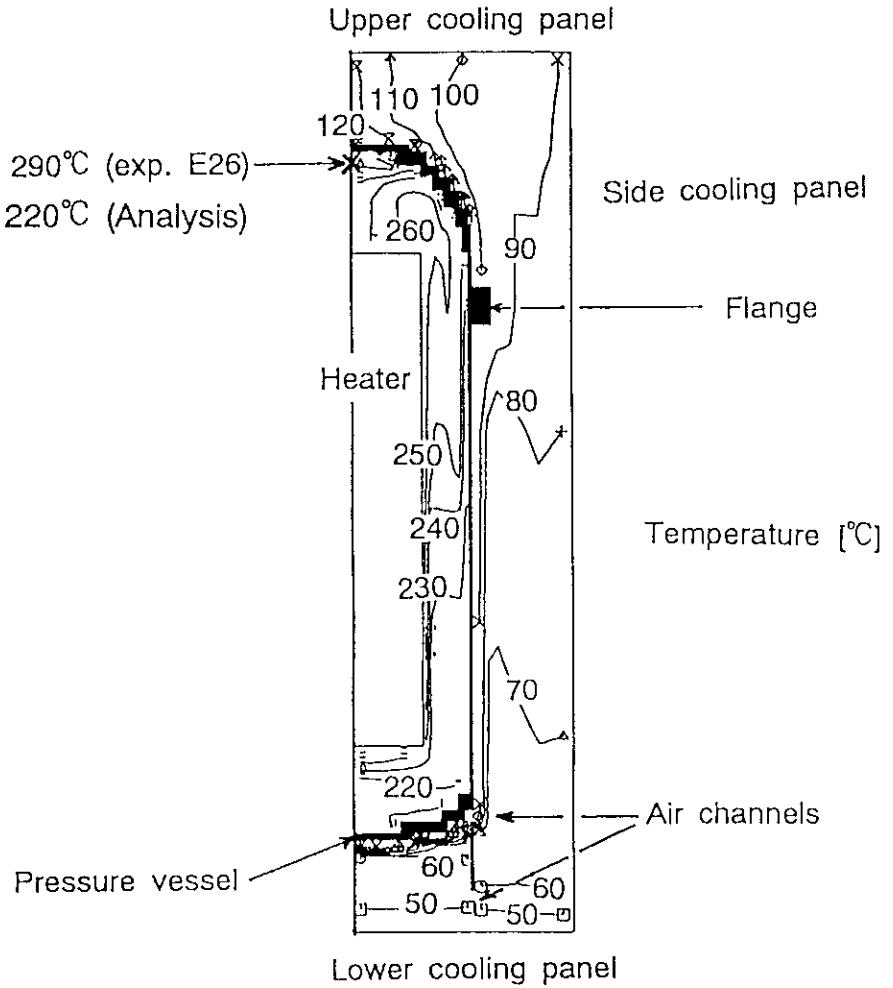

Fig.5.4(a) Analytical results of temperature contour
(Helium gas condition inside the pressure vessel)

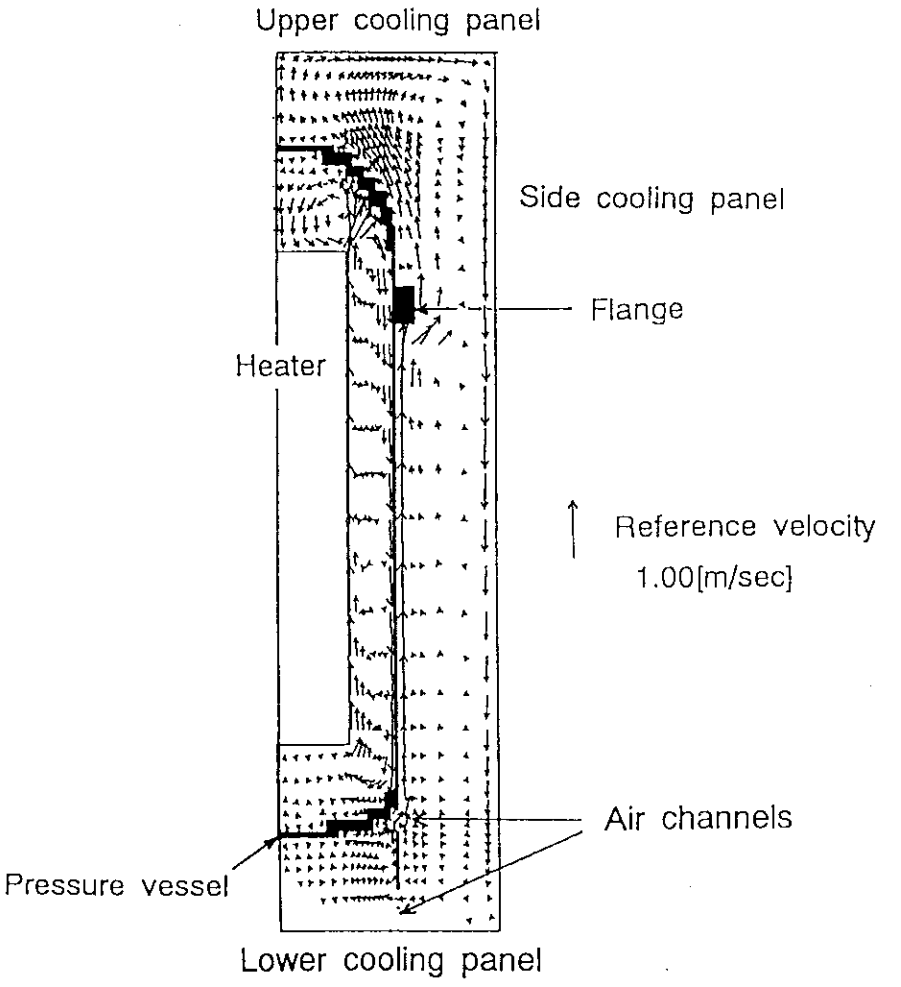

Fig.5.4(b) Analytical results of velocity vector
(Helium gas condition inside the pressure vessel)

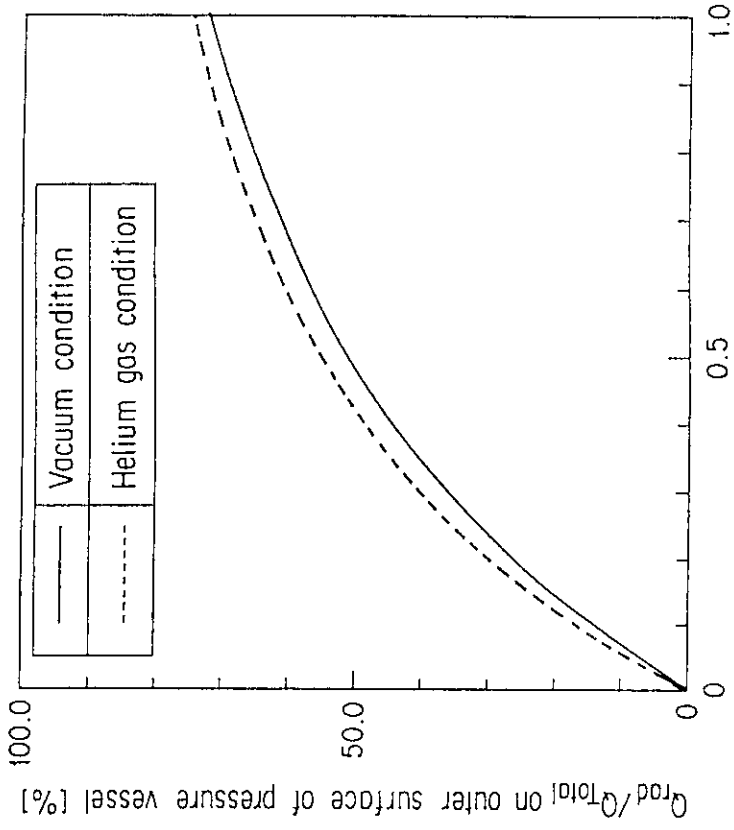

Fig.5.6 Relationship between emissivity and ratio of thermal radiation to total heat transferred to cooling panel

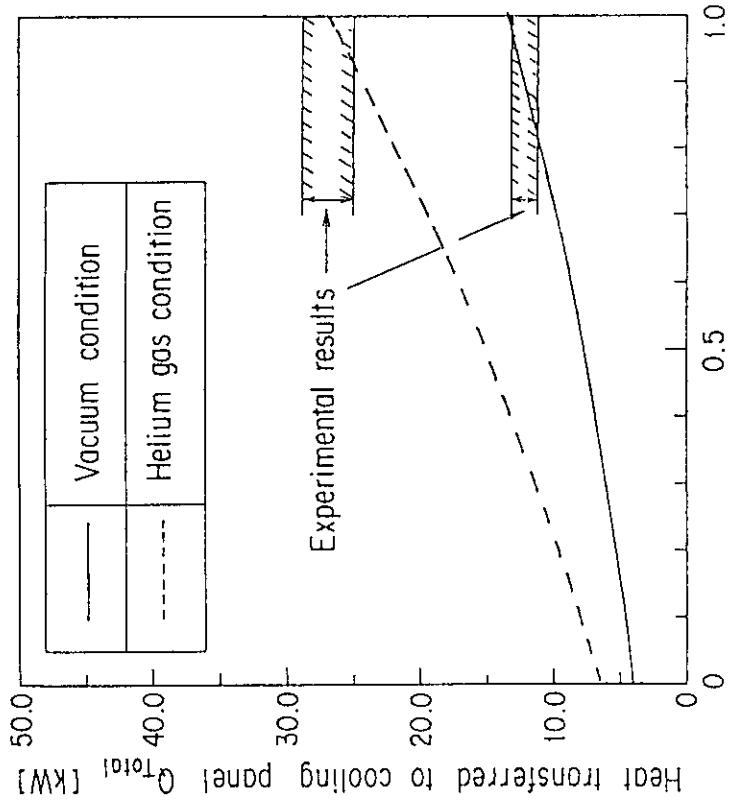

Fig.5.5 Relationship between emissivity and total heat transferred to cooling panel